Mechanistic Studies of Reactions at the Single-molecule Level Using Microfluidics with Applications in Molecular Diagnostics

Thesis by

Bing Sun

In Partial Fulfillment of the Requirements for the Degree of

Doctor of Philosophy

CALIFORNIA INSTITUTE OF TECHNOLOGY

Pasadena, California

2014

(Defended 05/02/2014)

© 2014

Bing Sun

All Rights Reserved

ACKNOWLEDGEMENT

First of all, I must thank my research advisor, Professor Rustem Ismagilov, who shaped the way I learn, think, and do things in science. Thank you for teaching me how to think critically and frame the problem correctly, for guiding me to perform research creatively and logically, for training me to describe science accurately and attractively. To me these capabilities are the most precious treasure I have acquired in graduate study. I am also grateful for him always being supportive as a mentor both in research and in my personal career.

I would like to thank my family, without the support of whom I would not have completed this phase of my life. To my dear parents, Wanfu and Bo, who have been sharing all the happiness and sadness together with me even when they were over 7,000 miles away. They taught me not only to stand firm and spare every effort to overcome difficulties before achieving the goal, but also to cherish the satisfaction of any small achievement. It was them who inspired my interest in science, especially in chemistry. To my grandparents, my uncles and aunts, and my lovely cousins, thank you for being an amazing family.

And thanks to all the colleagues at both UChicago and Caltech—starting from projects early on with Jason Kreutz to the last project with Jesus Rodriguez-Manzano, people were always friendly and helpful. I would like to dedicate my special thanks to Feng Shen, who led me into the productive track of research; to Toan Huynh, who gave me initial training on many instruments and influenced me with good scientific habits, and to Jesus Rodriguez Manzano, who brought so much fun to my last year in this lab. It was a real pleasure to work closely with people who were awesome project partners and fantastic friends: Jason Kreutz, Stephanie McCalla, David Selck, Mikhail Karymov, and Travis Schlappi—without them I could not have gone so far. To Rebecca Pompano, Elena Davydova, Liang Li, Weishan Liu, Liang Ma, Alexander Tucker-Schwartz, Stefano Begolo, Wenbin Du, and Daan Witters for providing all the generous help. To everyone

else in Ismagilov lab, for making it an exciting and creative place to work. I would like to thank especially Whitney Robles and Bridget Samuels who generously devoted time in editing my writing pieces, including this thesis.

I am also grateful to Professor Peter Dervan, Long Cai, Niles Pierce and Rustem for being on my committee for candidacy exam, proposition exam, and thesis exam. Thank you for your guidance and support for my graduate study here at Caltech.

ABSTRACT

Motivated by needs in molecular diagnostics and advances in microfabrication, researchers started to seek help from microfluidic technology, as it provides approaches to achieve high throughput, high sensitivity, and high resolution. One strategy applied in microfluidics to fulfill such requirements is to convert continuous analog signal into digitalized signal. The capacity to handle large amounts of small volume liquid enables the isolation of single entities into small compartments and the analysis of these single entities one by one in a “digitized” format. One most commonly used example for this conversion is digital PCR, which has been made commercially available. The idea of counting the number of reacted compartments (triggered by the presence of the target entity) out of the total number of compartments and using Poisson statistics to calculate the input amount of target is quite straightforward.

However, there are still problems to be solved and assumptions/conditions to be validated before the technology is widely employed. In this dissertation, the digital quantification strategy has been examined from two angles: efficiency and robustness. The former is a critical factor for ensuring the accuracy of absolute quantification methods, and the latter is the premise for such technology to be practically implemented in diagnosis beyond the laboratory. Although the discussion raises more challenges for digital assay development, it brings the problem to the attention of the scientific community for the first time. The analog-to-digital conversion concept does not only provide approaches for absolute quantification, but also offers a platform to perform mechanistic studies at the single molecule level. What the detail of the reaction scheme is and how each parameter influences the “fate” and “rate” of reactions at the single entity level could be understood using microfluidic platforms.

This dissertation also contributes towards developing POC test in limited resource settings. On one hand, it adds ease of access to the tests by incorporating massively producible, low cost

plastic material and by integrating new features that allow instant result acquisition and result feedback. On the other hand, it explores new isothermal chemistry and new strategies to address important global health concerns such as HIV detection and treatment monitoring as well as HCV genotyping.

TABLE OF CONTENTS

LIST OF ILLUSTRATIONS AND TABLES

CHAPTER 1

INTRODUCTION

1.1 Demand and challenge for point-of-care (POC) diagnostics in limited-resource settings

Diagnostics, defined as the process of attempting to determine or identify a possible disease, is a necessary step before treatment can be started. It plays an important role in global healthcare, in the sense that it does not only provide information for doctors to administer appropriate and timely care to patients, but also provides crucial surveillance data for public health strategies. The quality of a diagnostic test determines the accuracy of the test result and directly influences treatment decisions. Lack of access to high quality diagnostic tests or to even low quality diagnostic tests remains a huge problem in modern society, especially for the developing world or limited-resource settings.

The heavy burden of ill health caused by infectious diseases in the developing world is well recognized, where it accounts for over half of all deaths in children[1]. Malaria, acute respiratory infections, enteric infections, tuberculosis and HIV kill more than 10 million people each year, 95% of whom live in developing countries[1]. This number would have been smaller if early and reliable diagnostics were offered to patients at the initial stage of disease development and prompt treatments were adopted. However, people in the developing world usually have limited access to diagnostic platforms in centralized laboratories due to constraints in physical location or financial conditions. Clinical symptoms and local prevalence of a certain disease could be used occasionally as a rationale for beginning treatment, but it does not apply when diseases have no symptoms or have similar symptoms to other diseases[2]. As a result, the demand for easy-to-use, low-cost, transportable diagnostic platforms is a growing yet unmet need.

The criteria for an ideal diagnostic test for limited-resource settings has been set by the World Health Organization (WHO) Sexually Transmitted Diseases Diagnostics Initiative with the term

"ASSURED test", which stands for: Affordable by those at risk of infection, Sensitive (few false negatives), Specific (few false positives), User-friendly (simple to perform and requiring minimal training), Rapid (to enable treatment at the first visit), Robust (does not require refrigerated storage), Equipment-free, and Delivered to those who need it[3]. These criteria have captured the features of a good POC diagnostic test, by emphasizing both the availability and flexibility of such a test, as well as its accuracy. As is often the case, an assay with low complexity and cost, such as a lateral flow strip pregnancy test, does not offer as much and as accurate information as a sophisticated test, such as an assay involving quantitative polymerase chain reaction (qPCR). However, the complexity and cost of sophisticated tests is usually high, preventing them from being used as POC tests. How to reduce the complexity and cost without sacrificing the accuracy of the test is the first issue to consider before developing a new POC diagnostic test.

If categorized based on the target, POC diagnostic tests include protein assays, nucleic acid assays, human cell assays, metabolite and small molecule assays, and drug and food safety tests[4]. Examples include the prostate-specific antigen (PSA) test, C-creative protein (CRP) test, troponin I test for protein targets[4-5]; tests for human immunodeficiency virus (HIV), influenza, Methicillin-resistant Staphylococcus aureus (MRSA), and tuberculosis (TB) for nucleic acid targets[6]; and tests for cancer, inflammatory response and hematological parameters for whole cell assays[7]. Although some of the tests above have satisfied some criteria of an ASSURED test, most of them are still labor intensive or not cost-effective, especially quantitative assays.

Compared with regular detection assays, which only confirm the presence or absence of a target, quantitative assays often require higher complexity in assay design to measure the amount of target. The standard method for quantification is to monitor the progress of a reaction, the kinetics of which correlate to the amount of input target. As a result, a detection instrument with certain resolution is needed to measure the output signal, which sometimes is not easy to integrate into a

POC platform and cumbersome to operate by untrained users. One way to eliminate the need of such an instrument is to "translate" analog information into end-point digital information.

1.2 The concept of analog-to-digital conversion: two definitions

The definition of "digital" can be two-fold, as explained in a review by our group[8]: "the tendency to switch between discrete states in response to specific triggers", which is often described by "a sharp sigmoidal change between two states over a narrow range of input" (e.g., "off" or "on"); and the isolation of single entity from others, which enables the analysis of this target independently, unlike in a "bulk" format, where the overall output is influenced by interactions between molecules or reactions.

As such, the concept of "analog-to-digital" conversion also has two definitions: converting a system with a continuous signal intensity change to a system with only two distinct states, and converting a system with all targets present in the same environment to a system with each target separated from others and confined within its own environment. As distinguishing two discrete states has much lower requirements for resolution than resolving continuous intensity, the conversion from analog-to-digital for the first definition could facilitate the simplification of readout systems, which will be demonstrated in the next chapter with an enzyme-linked immunosorbent assay (ELISA) system. For the second definition, the amount of input target is directly reflected in the digitized pattern at the endpoint, eliminating the need for real-time monitoring of bulk reaction progress. The remainder of this dissertation focuses on the use of this concept in the quantification of nucleic acids and the identification of nucleic acid sequences.

1.3 Digitization can be realized on microfluidic platforms, using SlipChip as an example

Microfluidics, the manipulation of small volumes of liquid, provides a convenient tool for studying system at the single-target level. Many ways of achieving digitalization of targets have been reported such as moving droplets in micro channels[9], static droplets in compartments

controlled by valves[10], magnetic beads[11] and other delicate structures to capture single targets[12]. The high resolution and the ability to increase local concentration of generated product or secretion grants microfluidic devices significant advantages over other platforms.

SlipChip is a static droplet manipulation platform designed to operate multiple reactions simultaneously[13]. The SlipChip is composed of two pieces etched with ducts and wells (Figure 1). The two pieces are in close contact and sealed with lubricating oil. Through relative movement (slipping), the relative position of features on different pieces changes, resulting in the connecting and disconnecting of wells. In the “loading” position, fluid moves from the inlet through ducts and wells to the outlet; in the “isolating” position, the fluid stream is broken into discrete droplets inside each well; and in the “mixing” position, some droplets mix with other droplets pairwise when wells overlap. Reagents and samples can be loaded into different sets of wells, and kept separated until the device is slipped. SlipChip has been used to perform protein crystallization[14], immunoassays[15] and digital PCR[16].

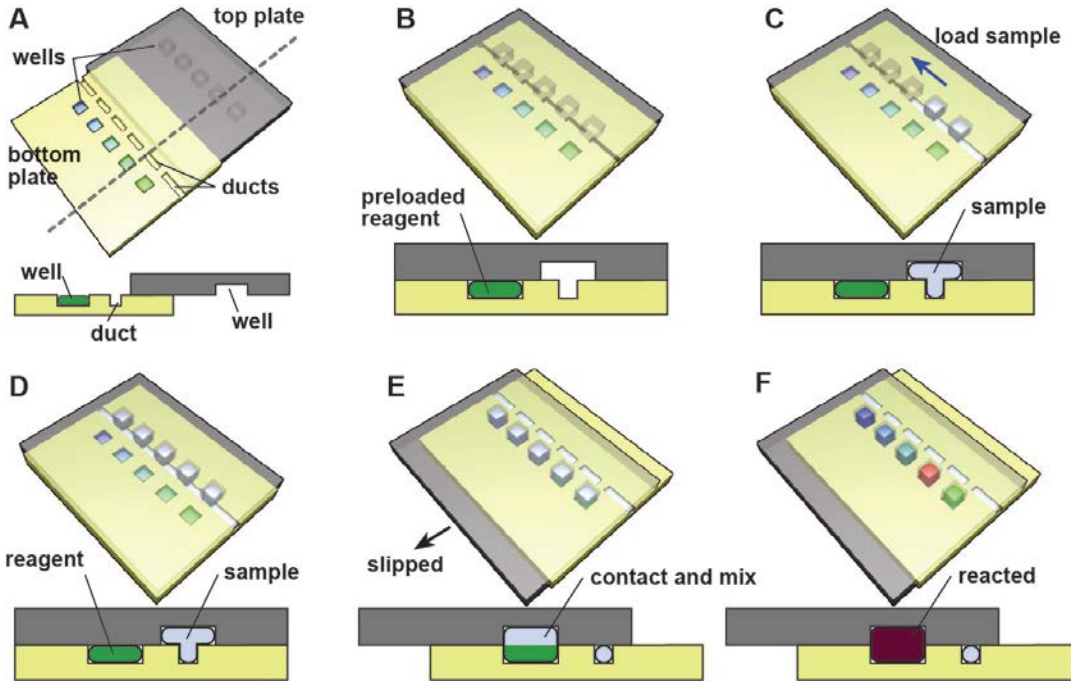

Figure 1 Schematic overview of fluid handling on SlipChip. (A) Off-set position of SlipChip, composed of a top plate and bottom plate, which are both etched with wells and ducts. (B) Assembled SlipChip at the "loading" position, where wells and ducts are connected. (C-D) The sample is loaded from inlet through the connected wells and ducts to the outlet. (E) Slipping-induced liquid stream to be broken into separate droplets and merged with preloaded reagent. (F) Reactions are triggered and different results are generated. Reproduced from reference 13 with permission of Royal Society of Chemistry.

Most of my graduate research involved the use of SlipChip microfluidic devices for the isolation and confinement of single molecules. In Chapter 2 of this dissertation the first definition of analog-to-digital conversion is described using the example of a threshold-enabled cystatin C quantification assay with visual readout on SlipChip. After the completion of that project, the focus of my research switched from protein to nucleic acid targets, and applied different nucleic acid amplification chemistries at the single-molecule level in a digital format for viral load quantification, which is described in Chapter 3 and 4. In these two chapters, strategies to allow large dynamic range and to eliminate thermal cycling are introduced to satisfy the requirements of limited-resource settings. To fully evaluate the performance of isothermal amplification chemistry, I tested the two major challenges for digital assays—efficiency and robustness, which are described in Chapter 4 and 5. Lastly, I expanded my research beyond viral load quantification

to genotyping, and developed a novel one-step isothermal assay for Hepatitis C Virus (HCV) genotyping, described in Chapter 6.

CHAPTER 2

CONVERTING ANALOG SIGNAL TO DIGITAL BY INTRODUCING THRESHOLD ENABLES VISUAL READOUT FOR A CYSTATIN C QUANTIFICATION ASSAY

2.1 Converting analog-to-digital readout using pre-determined thresholds

As discussed in the previous chapter, the amount of information one can extract from a test is usually correlated to the complexity of the test. Qualitative tests such as pregnancy tests require only endpoint yes/no readout and are relatively robust to changes in environmental conditions, but they do not give information regarding the quantity of the target. Quantitative tests usually require instruments to resolve continuous signal intensity at an endpoint, such as a fluorometer or Ultraviolet–visible (UV/Vis) spectrometer, or require kinetic measurements such as ELISA and qPCR. For protein target quantification, the most widely used methodology is still to measure the change in output (color, voltage, precipitation) over time. Simple and quantitative assays have been developed[17], but only with unsatisfactory resolution of an order of magnitude or higher.

We first asked the question of whether there is a way to convert the kinetic information to robust, reader-free endpoint information, and answered the question with the idea of "digitizing" the analog signal by introducing a threshold that inhibits the reaction with target concentration at or below a certain level[18]. Only when the target concentration exceeds the threshold will there be a positive reaction triggered by the excess target. By combining a series of ON (above threshold)/OFF (below threshold) bits, the concentration of target can be determined with the resolution set by the step size between thresholds. In the illustration given in Figure 2, a continuous analog signal is converted to a panel of digital bits that are either clear (ON) or colored (OFF). The input concentration can be determined by the position where bits transition from OFF to ON.

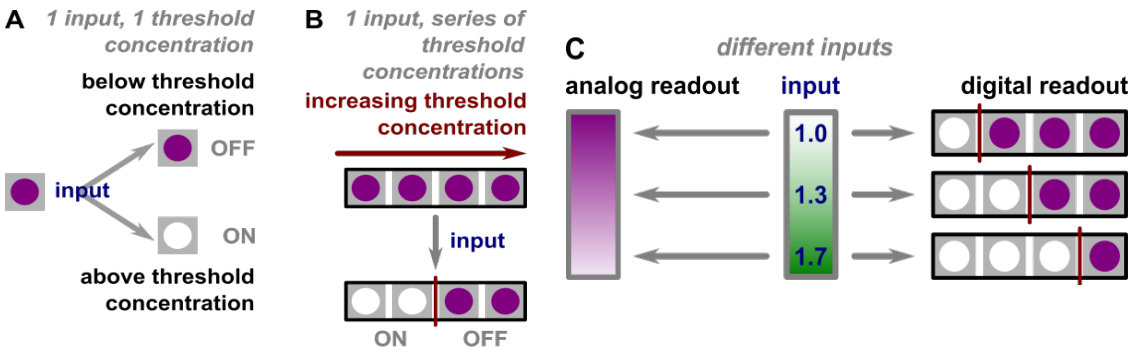

Figure 2 Illustration of analog-to-digital conversion based on thresholds. (A) ON (clear)/OFF (purple) of a single reaction depending on the relevant abundant of target to inhibitor. (B) A series of ON/OFF bits created by increasing threshold concentrations. (C) An illustration of analog readout versus digital readout. An analog readout gives a gradient change in intensity while a digital readout comprises a series of bits. Reprinted with permission from reference 18. Copyright 2013 American Chemical Society.

2.2 Applying the concept of threshold in the quantification assay of cystatin C

Glomerular filtration rate (GFR) describes the flow rate of filtered fluid through the kidney and is an indication of the state of kidney. Creatinine is the most widely used biomarker and its clearance rate is a useful measure for approximating the GFR. However, the level of creatinine varies with muscle mass and protein intake, and is not accurate at detecting mild renal impairment. A more accurate renal function indicator is the level of cystatin C, a low molecular weight protein removed from the bloodstream by glomerular filtration in the kidney. Its level is less dependent on age, gender, race and muscle mass compared with creatinine. It has been shown that cystatin C alone is superior to creatinine as a marker of kidney function in a meta-analysis[19], and adding the measurement of cystatin C to that of creatinine improves assay accuracy[20]. Therefore, here cystatin C is chosen as the model system to study. For cystatin C measurements, small changes as low as a 1.5 fold increase in concentration need to be detected[21].

The principle here is based on enzymatic inhibition: the enzyme (linked to the cystatin C molecule via antibody-biotin-avidin conjugate) is allowed to be bound by different amounts of inhibitor before reacting with substrate. For threshold positions with higher inhibitor

concentration than the enzyme concentration, all enzymes are inhibited and the reaction stays negative. For threshold positions with lower inhibitor concentration than the enzyme concentration, uninhibited enzyme will turn the reaction to positive. The concentration of available active enzyme increases dramatically near the threshold position with comparable inhibitor and enzyme concentration and thus changes the enzymatic reaction from negative to positive. The enzyme Acetylcholinesterase (AChE) can hydrolyze acetylthiocholine to thiocholine, which then turns the purple I_3^- /starch solution to clear (Figure 3). The assay was successfully performed with two samples from patients and four standard solutions (solution of purified cystatin C dissolved in cystatin C-free serum) and showed good agreement between experimental result and pre-quantified values.

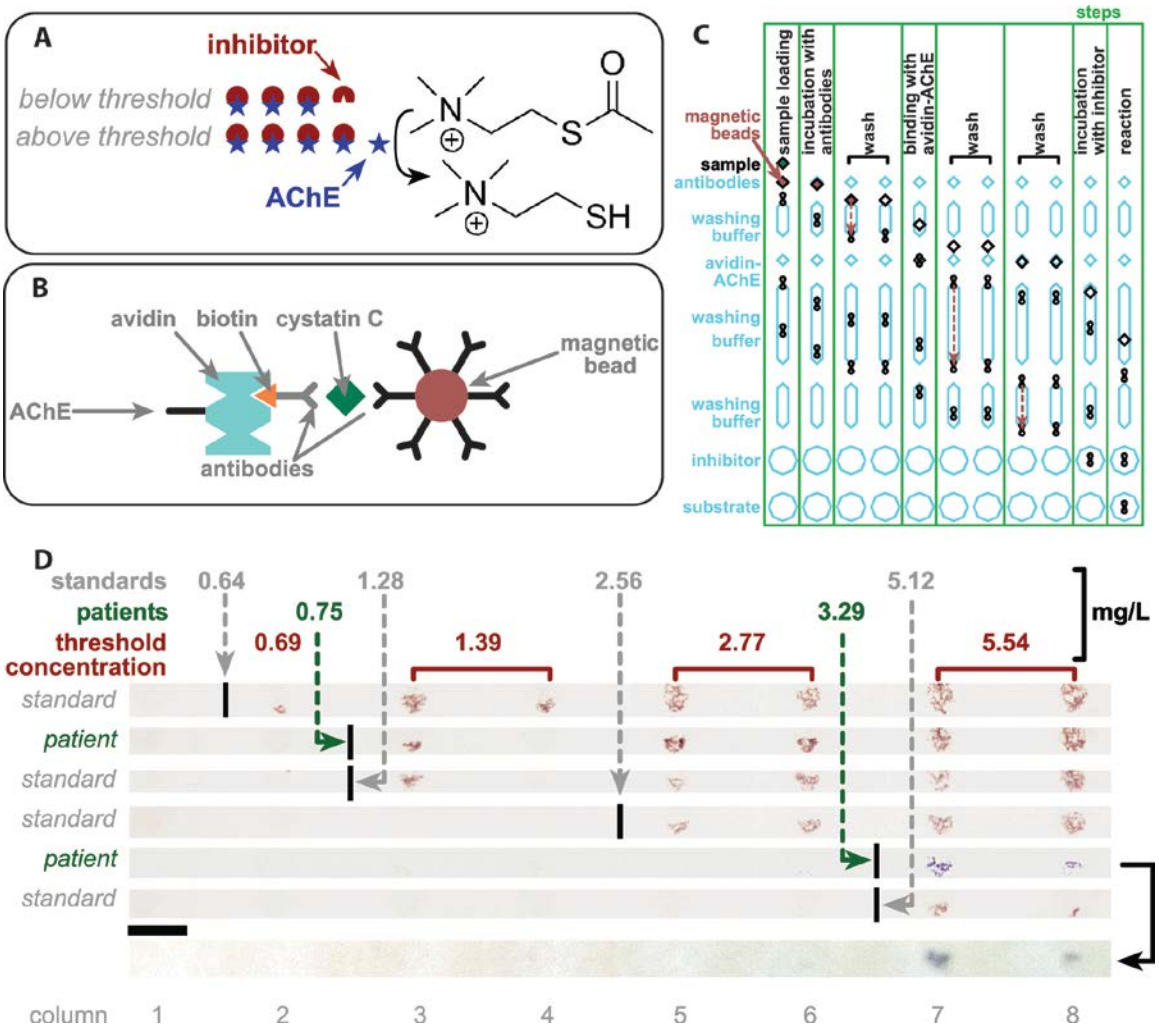

Figure 3 Schematic illustration and experimental results of the threshold-based cystatin C quantification assay. (A) A schematic drawing of the threshold chemistry and detection reactions. When the concentration of the enzyme AChE (star shape) exceeds that of the inhibitor (hemispherical shape), the enzyme hydrolyzes acetylthiocholine to give thiocholine. (B) A drawing of the complex used in the magnetic bead-based immunoassay for cystatin C, where cystatin C is conjugated with capture antibody on the magnetic bead and detection antibody linked to AChE via the biotin-avidin structure. (C) A drawing of the overall SlipChip design and assay procedures. One of the 12 columns is shown (11 times), illustrating the 8 steps of the assay controlled by the movement of the top (black) plate. The movement of magnetic beads is shown with red dashed arrows. (D) Photographs of results from standard solutions and clinical serum samples over a wide dynamic range, with each row corresponding to one assay (one SlipChip device). The very bottom row is a photograph of the result of the 3.29 mg/L patient sample taken by an iPhone 4 camera. Columns 3–4, 5–6, 7–8, 9–10, and 11–12 were set up as duplicates such that each pair contained the same inhibitor concentration. Scale bar: 2 mm. Reprinted with permission from reference 18. Copyright 2013 American Chemical Society.

2.3 Evaluation of the robustness of the threshold position to temperature variation

How an assay performs under various environmental conditions needs to be tested rigorously for any POC test. Here, we evaluated the robustness of the developed assay to changes in temperature and readout time (Figure 4). The temperature was controlled by a plate reader and the absorbance was measured periodically. To simplify the system, a chromogenic substrate, 5,5'-dithiobis-(2-nitrobenzoic acid) (DTNB), together with acetylthiocholine were adopted instead of the substrate used for visual readout, and the concentration of enzyme was kept constant when quantified with multiple thresholds determined by inhibitor concentration. We found that when the enzyme and inhibitor concentrations were higher (13 to 46 nM), the threshold was robust with a consistent contrast between ON and OFF reactions over a range of readout times (3-30 min), a range of temperatures (22–34 °C), and triplicates (Figure 4A). Reactions with inhibitor concentrations that were lower than the enzyme concentration gave ON results (13, 16, 21 nM), while the rest gave OFF results (27, 36, 46 nM). When the enzyme and inhibitor concentrations were lower (1.3 to 4.6 nM), even though the resolution was kept constant (1.3X change per threshold step), the working range of the assay became narrower. Increasing temperature shifts the enzyme/inhibitor equilibrium, and also influences the rate of the overall enzyme/substrate/DTNB reaction. The threshold position and working range depend on the combination of the two. In the case of high concentration, the two effects either cancel each other out or the influence is not significant enough; in the case of low concentration, the shift of equilibrium leads to the change in the threshold position.

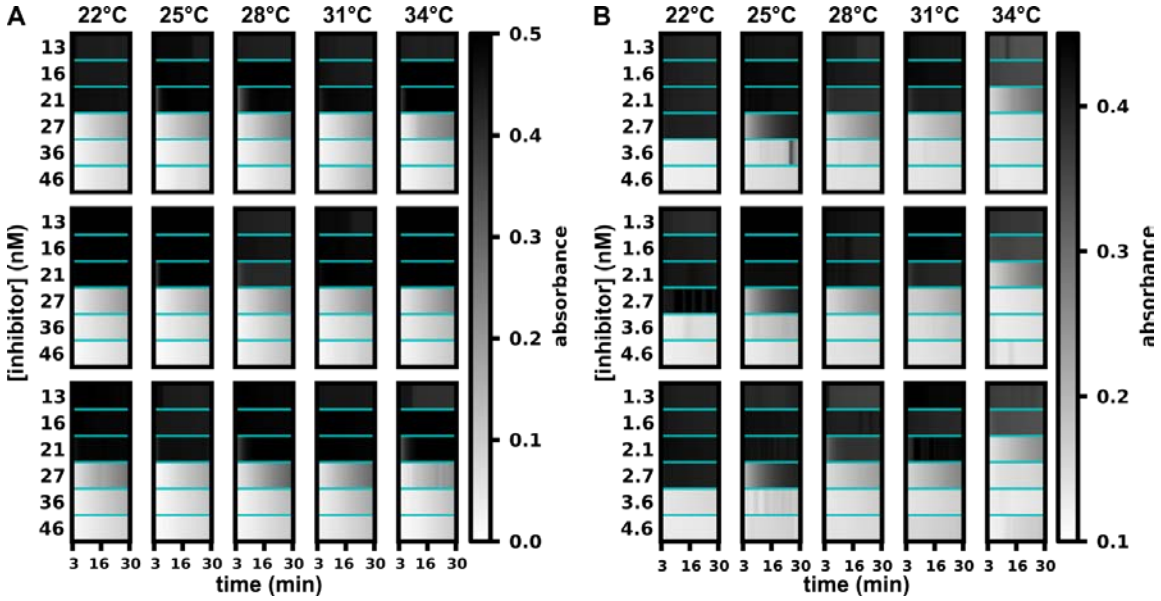

Figure 4 Robustness test results at different temperatures and reaction times for threshold chemistry. (A) False-color maps showing the results of threshold chemistry over a 1.3x dilutions of inhibitor concentration (13, 16, 21, 27, 36, and 46 nM) across a 12-degree range of temperatures (22 °C, 25 °C, 28 °C, 31 °C, and 34 °C). Three repeats are shown in different rows. (B) False-color maps showing the results of threshold chemistry over a 1.3x dilutions of inhibitor concentration (1.3, 1.6, 2.1, 2.7, 3.6, and 4.6 nM) across a 12-degree range of temperatures (22 °C, 25 °C, 28 °C, 31 °C, and 34 °C). Three repeats are shown in different rows. Higher absorbance stands for higher enzymatic activity. Reprinted with permission from reference 18. Copyright 2013 American Chemical Society.

This conversion from analog signal to digital signal using threshold chemistry enables the direct readout of a quantitative cystatin C assay in a reader-free manner, with high resolution (1.3X). This method can potentially be implemented into other clinical assays as well. The disadvantage of this chemistry lies in the fact that one assay is converted to multiple assays depending on the resolution requirement. However, microfluidics offers a solution, as it enables the parallel manipulation of many reactions, reducing the amount of sample used and the extra cost of integrating multiple assays.

CHAPTER 3

COMPARTMENTALIZATION GENERATES DIGITIZATION: USING DIGITAL PCR ON A MULTIVOLUME MICROFLUIDIC DEVICE TO QUANTIFY VIRAL LOAD IN A LARGE DYNAMIC RANGE

3.1 The need for viral load quantification and its challenges

Nucleic acid-based diagnostic tests detect the presence or determine the abundance of the DNA or RNA of the target in the host. Such tests are of particular interest in research ranging from early cancer diagnosis, to prenatal diagnosis, to infectious disease detection and genotyping. In all of these cases, nucleic acids carry important information. Viral load quantification, defined as measuring the amount of virus present in 1 mL bodily fluid, is critical for monitoring the progression of the viral infection and the outcome of the performed treatment. One of the examples is the need for HIV viral load monitoring during treatment. Nowadays, first-line antiretroviral treatment for HIV patients is becoming more available, which increases survival time. However, it begins to fail when several key mutations in the HIV genome appear and drug resistance develops. To ensure prompt responses to such failures and to stop the spread of drug resistance, it is recommended to measure HIV viral load regularly. HIV viral load test should not only have high resolution (2-3 fold), but also large dynamic range (50 copies/mL to 750,000 copies/mL). HCV, one of the major causes for liver disease and cirrhosis, is another example where viral load information is required to determine therapy and monitor treatment outcome. Although the requirement for resolution for HCV (1 log) is lower than that of HIV, it requires a larger working range: the viral load for chronic HCV ranges from 50,000 to 5 million international unites per mL (IU/mL)[22], and for patients taking antiviral therapy it can go down to 50 IU/mL. Similarly to many other infectious diseases, the majority of the HIV- and HCV-infected population live in the developing world or limited-resource settings. Therefore, a POC viral load quantification assay with large dynamic range and high resolution is in demand.

3.2 Digital PCR quantifies nucleic acid by converting analog signal to digital

Most nucleic acid-based quantitative tests are performed in central laboratories with real-time PCR. However, this method is cost-prohibitive under limited-resource settings and usually requires multiple instruments, highly skilled technicians, and isolated rooms. Digital PCR on simple microfluidic devices presents an alternative quantification method in non-laboratory settings. In digital PCR, single nucleic acid molecules are separated into compartments and amplified independently. An absolute count of the target molecule is obtained at the endpoint, eliminating the need for real-time monitoring.

Digital PCR is one example of the second definition of "analog to digital conversion" discussed in Chapter 1. By isolating single entities from each other, the amplification of each molecule proceeds without interference from other molecules, and the rate of reaction does not influence the quantification result as long as the final state of a reaction can be clearly recognized as ON or OFF. Based on the digital pattern (number of ONs and OFFs) acquired at the end of the reaction, the amount of input molecule could be calculated based on Poisson statistics. Poisson and binomial analysis can be used to quantify number of input molecules based on the number of negative wells. The details of equations derived from Poisson distribution in the context of digital PCR have been reported before[23] and can be found in Appendix F. Although digital PCR has been demonstrated on various platforms, including well plates[24], microdroplets[25], spinning disk[26] and Openarray[27], most of them still require complicated manipulation systems. SlipChip, which relies only on simple slipping to manipulate droplets on device, offers an easy platform to perform digitization[16]. Digital PCR has been successfully performed on SlipChip using *S aureus* gDNA (Figure 5) and the quantification results agreed well with spectrophotometry measurement results.

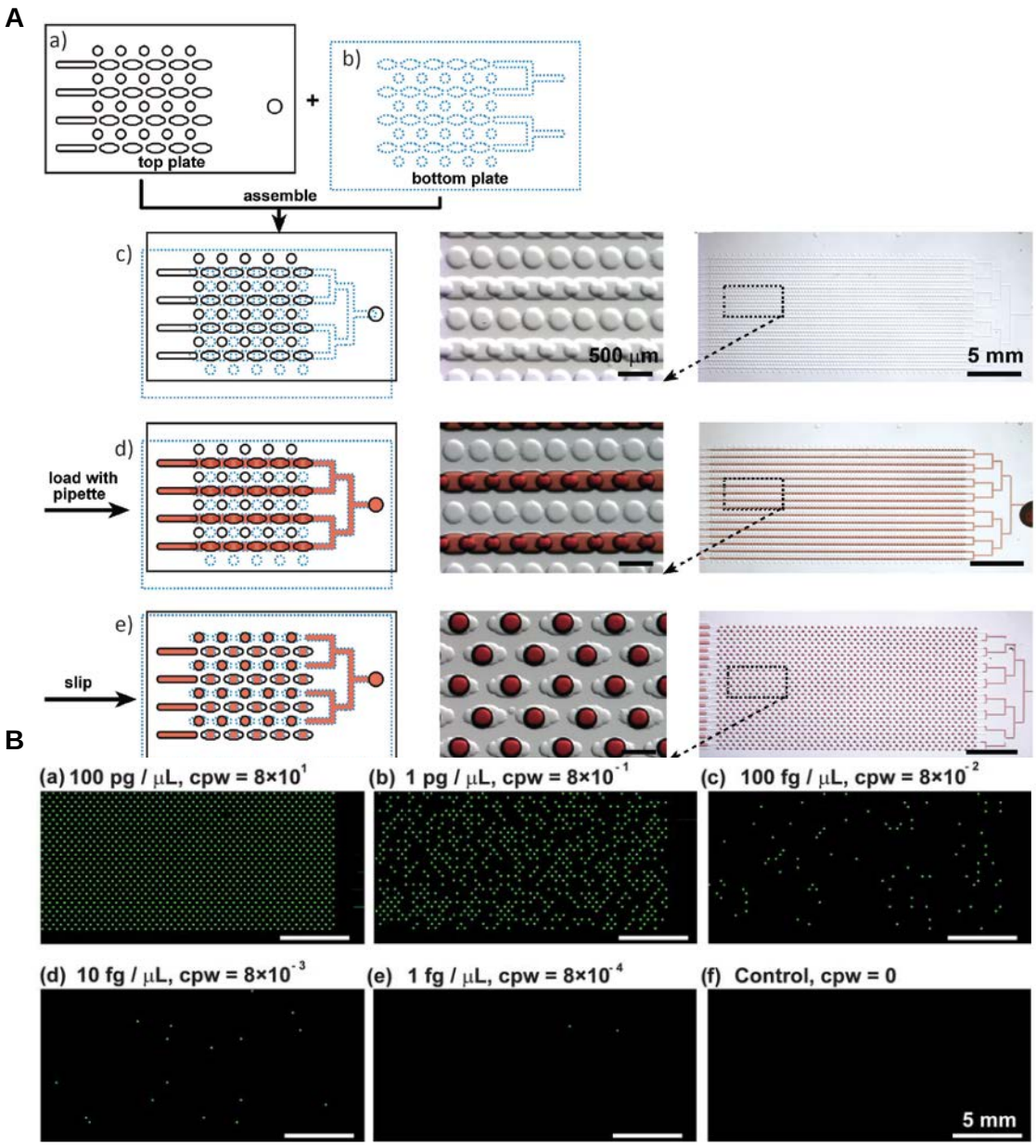

Figure 5 Schematic drawing and bright field image of SlipChip used in digital PCR assay and the fluorescence image of digital results. (A) Schematic overview of the design and mechanism of SlipChip for digital PCR. Black solid line depicts the top piece (a) and blue dotted line depicts the bottom piece (b). The two pieces are assembled and the aligned such that the elongated wells in the top and bottom plates overlapped to form a continuous fluidic path (c). The aqueous reagent (red) is injected into SlipChip and flows through the connected elongated wells (d). The two pieces are slipped relative to each other to the position where the fluidic path breaks up and isolated droplets form (e). (B) Digital PCR on the SlipChip with different concentrations of *S. aureus* gDNA. a-f) Digital PCR on the Slipchip with a serial dilution of target DNA template ranging from 100 pg/μL to 0 fg/μL. Reproduced from Reference 16 with permission of The Royal Society of Chemistry.

3.3 Using a combination of multiple volumes to achieve large dynamic range

Typical digital PCR platforms including the SlipChip design discussed above use wells of the same volume. The upper limit of quantification is determined mainly by the volume of each well and the lower limit of detection is determined by the total volume analyzed on the device. Therefore, in order to achieve a large dynamic range, a large number of wells need to be used. How to achieve the largest dynamic range with the least material and space possible remained a challenge. Our solution was to combine wells of different volumes on the same device. The smallest wells enable quantification of the target at high concentrations while the large volume wells contribute to the quantification of the target at low concentrations. This multi-volume approach can achieve the same dynamic range as single-volume approaches without the need for an excessive number of wells[23]. Careful consideration in the mathematical treatment when combining results from multiple volumes has been given[23] and the analysis was successfully applied in the quantification of HIV and HCV RNA[28].

The performance of digital RT-PCR in a multivolume digital SlipChip was first characterized with a 6 log serial diluted synthetic RNA (Figure 6). As the RNA concentration increased, the place where “digital” pattern was observed started to shift from the larger volume to the smaller volume. The calculated experimental results across the concentration range agreed well with the theoretically predicted distribution and 74% of the experiments fell within the 95% confidence interval.

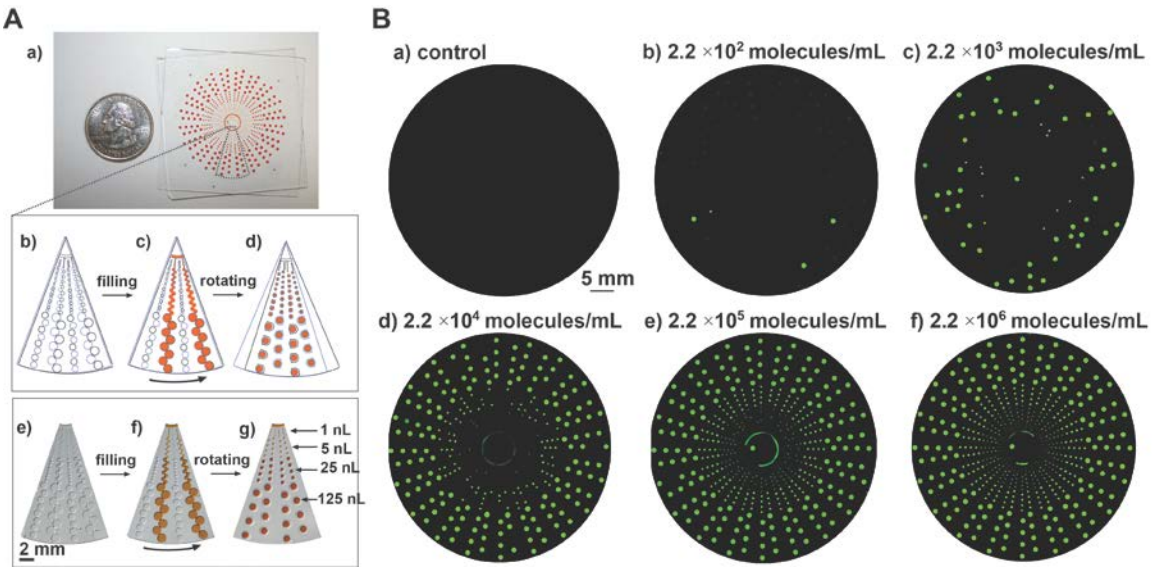

Figure 6 Schematic drawing and bright field image of multivolume SlipChip device and the fluorescence image of assay results (A) The bright field image (a, e-g) and schematics (b-d) of the rotational multivolume SlipChip (well volumes: 1nL, 5nL, 25nL, 125nL). The dead-end filling process was shown step-by-step: (b,e) SlipChip at the loading position; (c,f) orange food-dye was loaded along the connected wells; (d, g) after rotational slipping, droplets of four different volumes were formed simultaneously. (B) A serial dilution of the synthetic RNA on rotational multivolume SlipChip from 0 to 2.2×10^6 molecules/mL in the RT-PCR mix. Reprinted with permission from reference 28. Copyright 2010 American Chemical Society.

3.4 Running multiplex assays while maintaining large dynamic range on a multivolume SlipChip

To perform multiplex assays on the same device, wells need to be divided into different sections and therefore the dynamic range of each section will be decreased. To maintain the large dynamic range for each section, another two sets of volumes (0.2 nL and 625 nL) were added to the design described previously. When the entire device was used for one assay, the lower detection limit was improved from 120 copies/mL to 40 copies/mL, and the dynamic range was improved from 5.2×10^2 - 4.0×10^6 copies/mL to 1.7×10^2 - 2.0×10^7copies/mL. The lower detection limit of the new design was tested with a pre-quantified HIV RNA with an expected concentration of 51 copies/mL. With the new multiple volume design, the concentration was determined to be 70 copies/mL with a standard deviation of 20 copies/mL based on the analysis of six experiments (a representative image is shown in Figure 7C), which agreed well with the predicted value.

To test the compatibility of this device with multiplexed assays, the design was modified to divide the wells into five sections for five different samples, which can be injected into SlipChip simultaneously by pressure (Figure 7A). The lower limit of detection for each sample is 2.0×10^2 copies/mL and the dynamic range is 1.8×10^3 to 1.2×10^7 copies/mL. The multiplex SlipChip device was tested with HIV and HCV RNA to mimic the scenario of a patient with HIV/HCV co-infection (Figure 7B). The 5 samples applied were: HIV viral RNA, HCV viral RNA, negative control for HIV, negative control for HCV and a synthetic control RNA to determine the sample preparation recovery rate. Digital RT-PCR was performed with all the samples using the same thermal cycling profile. No cross-contamination or false positives were observed in the panel. The measured concentration of HIV RNA was 1.2×10^6 molecules/mL with a standard deviation of 3.7×10^5 molecules/mL in the original plasma sample, while the predicted concentration was 1.5×10^6 molecules/mL. The measured concentration of HCV RNA was 2.3×10^7 molecules/mL with a standard deviation of 9.7×10^6 molecules/mL in the original plasma sample. Based on this result, the conversion factor from international units (IU) to copy number for HCV viral load in our test was determined to be approximately 0.9, which was the same as the number published for the Roche Amplicor HCV Monitor v2.0 test when using a manual purification procedure[29].

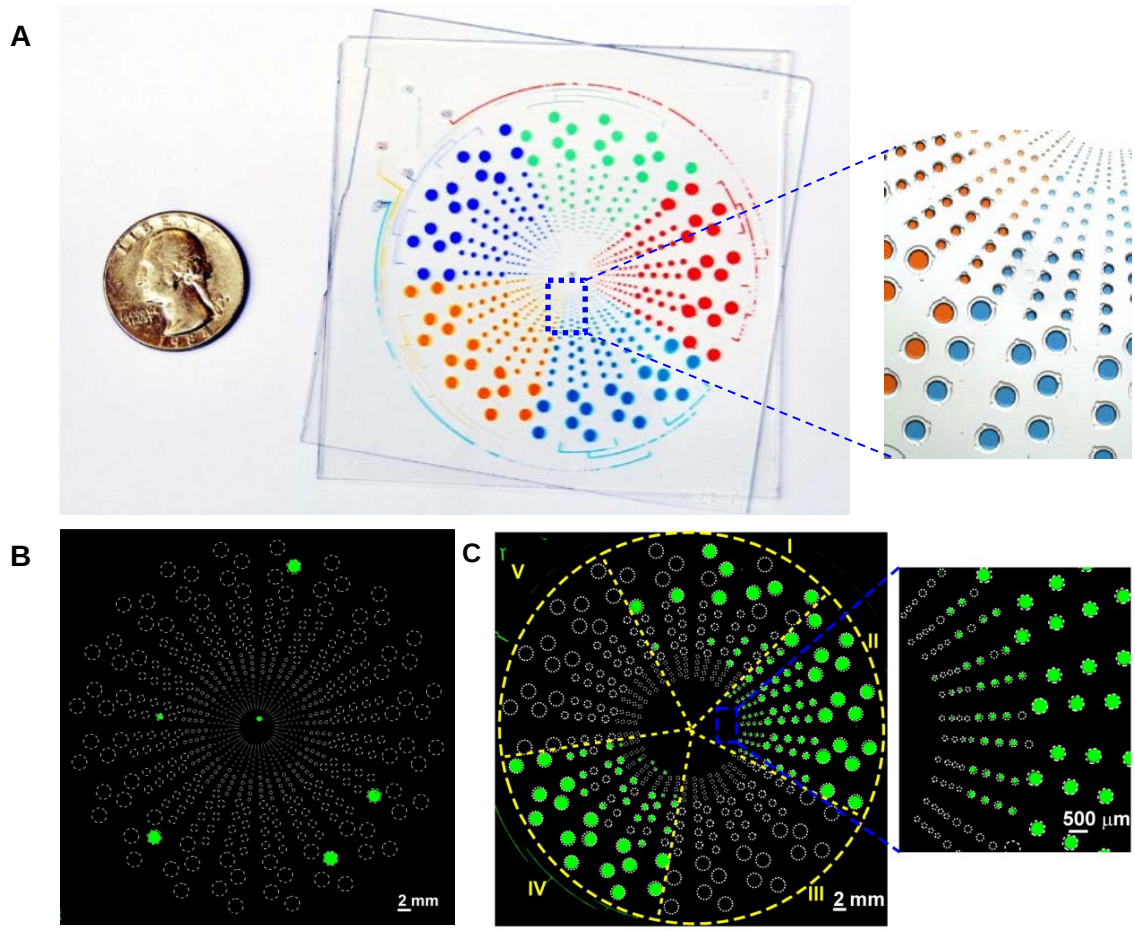

Figure 7 Bright field image of multiplex format multivolume SlipChip and the fluorescence image of assay results. (A) A photograph of a multiplex SlipChip device for 5 different samples (shown in different colors). Inset shows a zoomed-in area at the edge between two samples. (B) Representative experiment performing RT-PCR of HIV viral RNA at an expected concentration of 51 molecules/mL to test the lower detection limit of the device. This experiment was repeated six times to quantify the viral RNA concentration. (C) Fluorescence image of a multiplexed digital RT-PCR detection panel with 5 sections: I-V) measurement of control RNA in HCV sample, HCV viral RNA; negative control for HIV; HIV viral RNA; negative control for HCV. Inset shows an amplified area from HCV viral load test. Reprinted with permission from reference 28. Copyright 2010 American Chemical Society.

The multiplexing capability enables easy incorporation of necessary control experiments in the same assay and simultaneous monitoring of multiple targets, such as co-infection diseases and genotyping. The multivolume multiplex device also allows flexibility of using the same device to perform multiple assays of lower quality or single assays with higher quality depending on the application. Such a platform could be valuable in various applications besides viral load

quantification, such as detection of rare cells or rare alleles and prenatal diagnostics due to its high sensitivity. The rotational format is suitable to be applied in resource-limited settings because of the ease of operation.

CHAPTER 4

FROM THERMAL CYCLING TO ISOTHERMAL: CHALLENGES FOR EFFICIENCY

4.1 Eliminating the need for thermal cycling using isothermal amplification

Although digital PCR has been studied and incorporated in various molecular diagnostic assays[16, 25-27], the requirement of thermocycling limits its application in non-laboratory settings. Isothermal nucleic amplification technologies, which use a constant temperature during amplification, reduce the cost and complexity of the instrument, and therefore are more suitable for limited-resource settings. A water bath or very simple chemical heater could be used as the heating source[30]. Many isothermal amplification methods have been invented, including Nucleic Acid Sequence Based Amplification (NASBA) [31], Signal Mediated Amplification of RNA Technology (SMART) [32], Helicase Dependent Amplification (HDA) [33], Loop Mediated Isothermal Amplification (LAMP)[34], Recombinase Polymerase Amplification (RPA) [35], Rolling Circle Replication (RCA) [36], Strand Displacement Amplification (SDA) [37], Exponential Amplification Reaction (EXPAR)[38], Nicking Enzyme Amplification Reaction (NEAR) [39], and DNA circuits[40]. The underlying principles for each amplification chemistry differ, but the key issue for isothermal amplification chemistry is how to generate single-stranded DNA (ssDNA) or ssRNA that allows further annealing of the primer and elongation initiated by the primer to form new strands. This can be achieved by many means, such as with enzyme-assisted double strand opening, strand displacement, and RNA transcription. However, to be applied in a POC test, the reaction should have some other features, including low rates of false positives and false negatives, low requirements for storage conditions, and functionality without complicated instruments for signal readout.

4.2 Loop mediated isothermal amplification (LAMP)

LAMP chemistry is a widely adopted isothermal amplification method that requires constant reaction temperature at 60-65 °C and the participation of only one enzyme (*Bacillus*

stearothermophilus DNA polymerase). LAMP amplifies DNA with high specificity, efficiency and rapidity[34]. It employs a set of four or six specially designed primers that target six or eight distinct regions on the DNA sequence (Figure 8), which guarantees high specificity. The primers are designed in such a way that primer annealing and extension trigger strand displacement, which further produces single-stranded loop structures, allowing further primer annealing and strand displacement (Figure 8). The existence of multiple loop structures on the same amplicon strand significantly increases the number of nucleotides being incorporated per primer annealing event, resulting in the generation of a large number of pyrophosphate as the byproduct of DNA synthesis. Therefore, a calcein-metal based detection chemistry can be used to indicate the accumulation of pyrophosphate during the reaction. This detection chemistry enables the readout of reaction results with a simple image device such as a cell phone or even the naked eye[41]. In summary, LAMP or its derivative RT-LAMP method is a good candidate for the amplification chemistry used in POC molecular diagnostic tests.

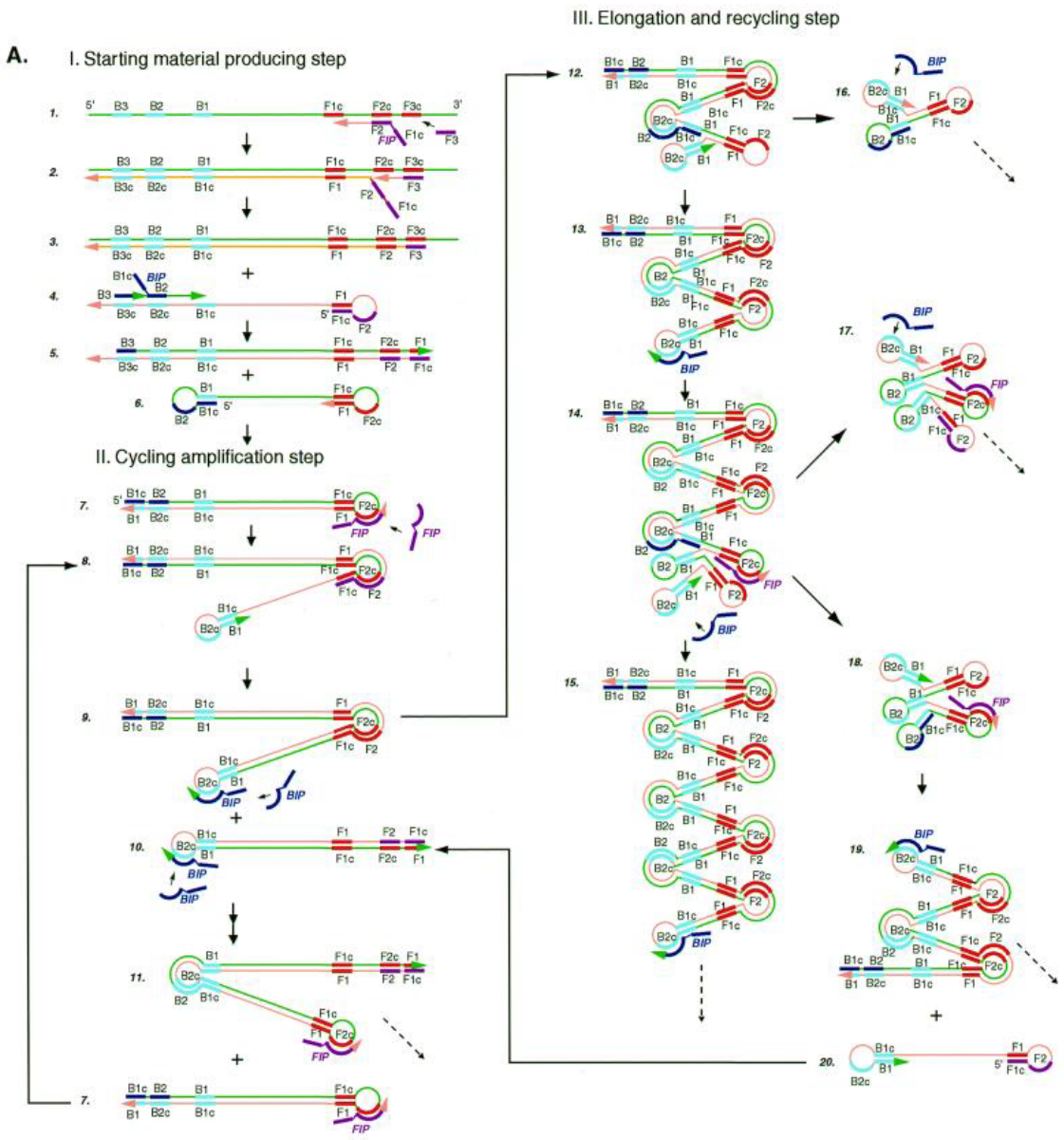

Figure 8 Schematic representation of the mechanism of LAMP. Steps of LAMP reaction are separated into: I) starting material producing step where the double looped structure is generated; II) cycling amplification step and III) elongation and recycling step. Reproduced from reference 34 by permission of Oxford University Press.

4.3 A problem to be carefully evaluated for digital amplification: efficiency

Here we use RT-LAMP for HIV RNA quantification as a model system to answer the question of whether digital RT-LAMP is an attractive alternative to real-time RT-PCR for quantitative diagnosis in limited-resource settings[42]. Although digital LAMP has been demonstrated previously with dsDNA target[43], digital RT-LAMP has never been reported before. The reverse transcription step is necessary when targeting a variety of infectious disease, but could potentially add complexity and introduce issues. We found that performing digital RT-LAMP in a single step on SlipChip is indeed problematic for quantifying HIV viral RNA: the quantification result using digital RT-LAMP was only 2.0% of that achieved using digital RT-PCR with the same template concentration. In this experiment, we compared quantification results of HIV viral RNA at four dilutions using two different digital chemistries—digital RT-PCR and digital RT-LAMP. Digital RT-PCR with primers targeting the LTR region of HIV was used as the standard because it has been validated previously[28]. For RT-LAMP, we used a commercial kit and a set of primers targeting the p24 gene modified based on previous publication[44]. We observed dilution curves with good linearity for both digital chemistries listed above; however the absolute values were dramatically different: the same concentration of RNA gave quantification values that differed by ~50 fold, with digital RT-LAMP giving lower digital counts. We also performed digital RT-PCR with B3/F3 primers taken from the LAMP primer set for comparison and found that even with the same amplification chemistry, the quantified value still differed by 2 fold, with B3/F3 primers giving lower digital counts.

To facilitate the discussion, we defined the percentage of amplified molecules out of the total number of input molecules as “efficiency”. Because digital quantification relies on counting the absolute number of molecules, one essential assumption is that every molecule gets amplified. In other words, people always assume that the efficiency is 100% for digital quantification, which has been shown to be not true in our case. Digital quantification methods with low efficiency,

such as digital RT-LAMP and digital RT-PCR with B3/F3 primers, will not give accurate results and will be inadequate for quantifying lower concentrations of analytes. This is a problem, especially in the case of HIV viral load, where changes most often in the range of 50 to 5,000 copies of RNA per mL need to be quantified to make clinical decisions.

4.4 Improving efficiency by separating sequential reactions from one another

To understand the mechanism leading to this inefficiency, we tested a few hypotheses and devised a way to address the problem to a considerable extent. We hypothesized that the RT-LAMP reaction consists of two stages: initiation before a dumbbell-shaped ssDNA is formed (Figure 8) and propagation after the cycling amplification starts. We hypothesized that the propagation step does not influence the efficiency, but only the time required for the amplification to go to completion; therefore it is the initiation stage that is critical in determining the efficiency. We designed experiments to test which stage determined the efficiency of amplification and validated the hypothesis. Here, the digital format enables us to see this "efficiency" directly reflected as the count of amplification and to separate part of the initiation stage from the other steps. To decouple the reverse transcription step from the amplification step, we designed a SlipChip device to perform RT-LAMP reaction in two steps (Figure 9).

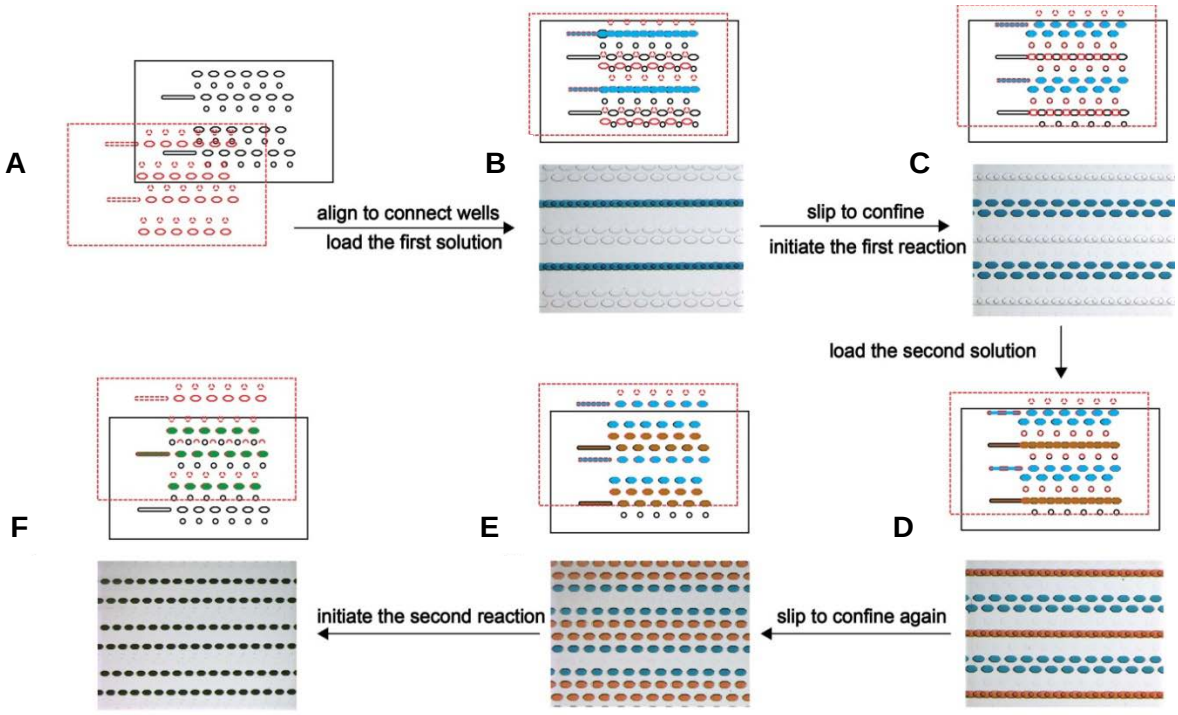

Figure 9 Schematic drawings and bright field images describing the operation of SlipChip for two-step digital experiments. A) Top piece (black) and bottom piece (red) facing each other before assembly. B) The two pieces were aligned to connect ducts and wells. Solution 1 (blue) was introduced along the connected channel. C) Slipping caused the fluid stream to break and isolated droplets were generated and confined in each well. The first step of reaction could be triggered at this stage. D) A second solution (orange) was loaded from another inlet along another set of connected wells and ducts. E) An additional slip generated isolated droplets. F) The two solutions were mixed on the device and the second step of the reaction was triggered simultaneously for all molecules. Reprinted with permission from reference 42. Copyright 2013 American Chemical Society.

With the two-step SlipChip device, we evaluated the influence of several factors in the reverse transcription step, including the orders of primers annealing and the property of different enzymes. We found that when the following changes were made, the efficiency was improved by 10 fold (Figure 10A): 1) only having BIP primer in the first RT step to exclude the interference of other primers; 2) replace AMV reverse transcriptase with Superscript III reverse transcriptase; 3) adding thermostable RNase H in the second step.

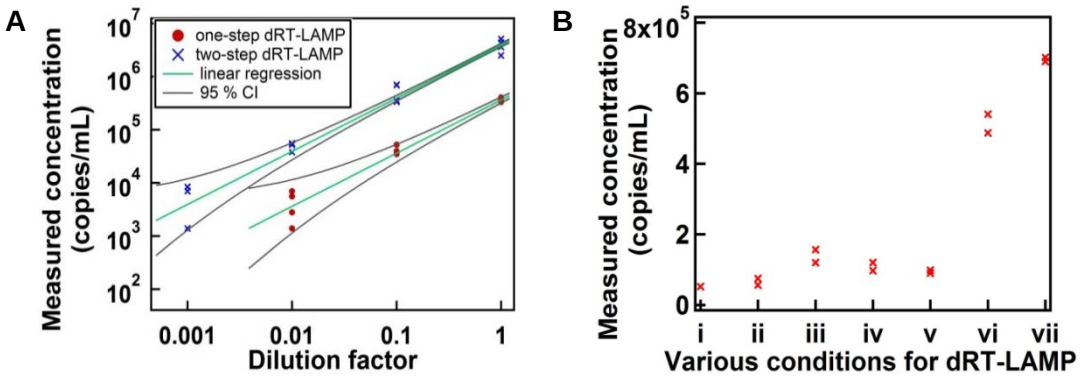

Figure 10 Quantification results of HIV viral RNA concentration (copies/mL) with digital RT-LAMP using different protocols. (A) Quantification results of HIV viral RNA (copies/mL) in a serial dilution experiment on SlipChip using one-step digital RT-LAMP and two-step digital RT-LAMP (n=4). Error bars represent standard deviation. (B) i-vii: one-step digital RT-LAMP; two-step digital RT-LAMP, all primers in RT step, AMV RT; two-step, BIP in RT step, AMV RT; two-step, BIP in RT step, Superscript III; two-step, BIP in RT step, AMV RT, with RNase H; two-step, BIP in RT step, Superscript III, with RNase H; and two-step, BIP in RT step, Superscript III, with RNase H, 0.5x calcein (n=2). Reprinted with permission from reference 42. Copyright 2013 American Chemical Society.

We first hypothesized that if instead of BIP primer, LOOP_B or B3 primer hybridize first to the RNA target and initiate reverse transcription, they would hinder the formation of looped structures on the B side. To test this hypothesis, we tested the efficiency when only BIP primer was present in the first step versus the efficiency when all primers were present, and found a 2 fold higher efficiency for the former. We then evaluated the performance of two different reverse transcriptases to see if the property of the enzyme played a role here. It was found that replacing the AMV reverse transcriptase with Superscript III, which has been reported to have a higher yield, led to no efficiency change. However, when RNase H was added to the second solution, the efficiency improved to 25% (Figure 10B). This could be attributed to the lack of RNase H activity and strand displacement activity in Superscript III—although it synthesized more cDNA, the release of cDNA was prevented.

To exclude the influence of the reverse transcription step, we performed digital LAMP assay with a synthetic 225 nucleotide ssDNA of the same sequence as the HIV RNA as template. The hypothesis behind this was that if the formation of desired cDNA was no longer the bottleneck,

digital LAMP using ssDNA as the template would have the same efficiency as two-step digital RT-LAMP starting from HIV RNA. The experiment results agreed with our expectation: the efficiency was quite similar between digital RT-LAMP for HIV RNA (39%) and digital LAMP for ssDNA (33%) compared to digital RT-PCR with B3/F3 primer, which indicated that the reverse transcription is not the efficiency-limiting step in the two-step protocol. Based on the experimental observation above, we proposed a new mechanism as shown in Figure 11.

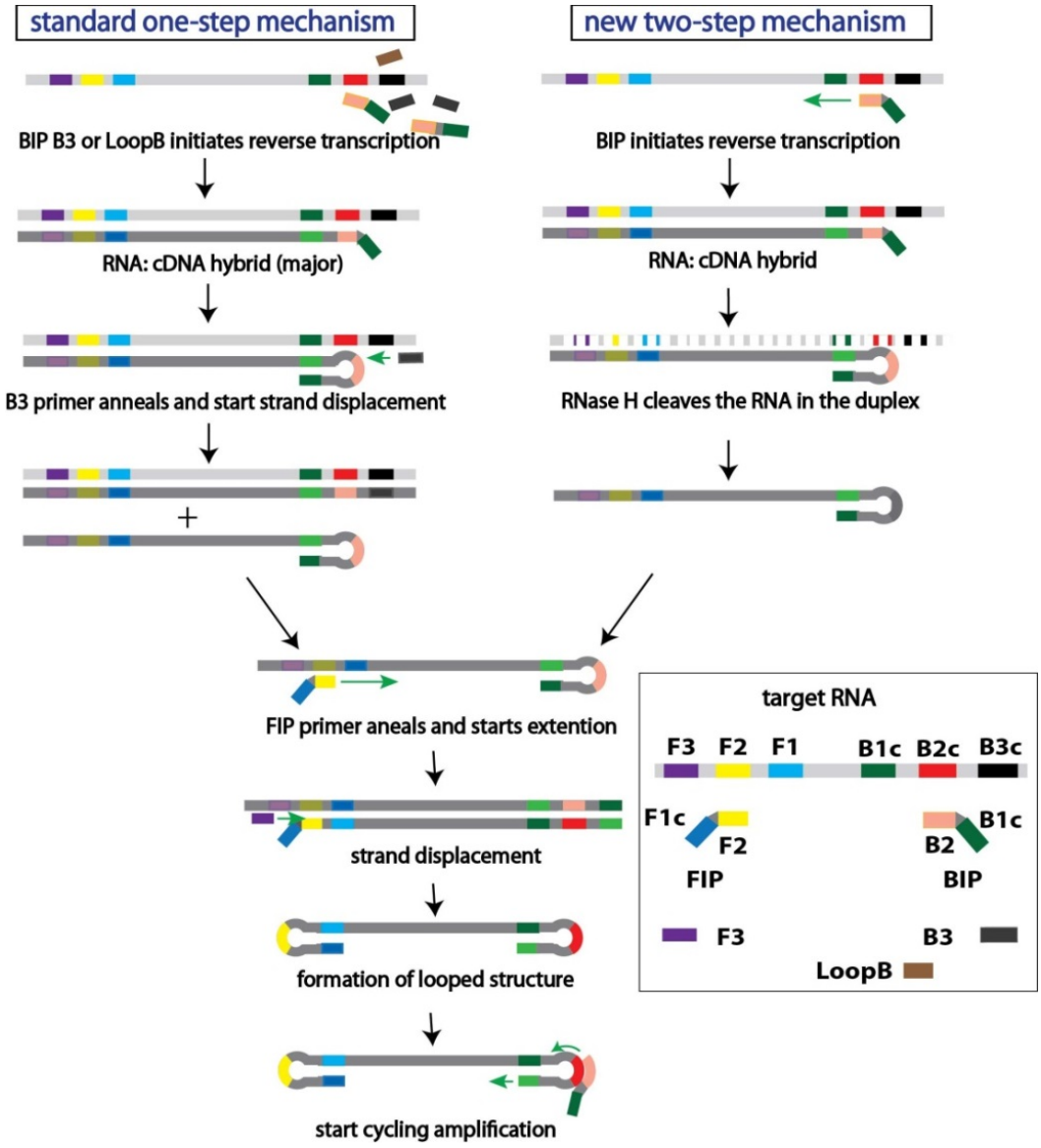

Figure 11 A comparison of the new two-step RT-LAMP mechanism and the published one-step RT-LAMP mechanism. In the initial step, the two-step mechanism uses only BIP primer, while the one-step protocol uses all primers together. After the formation of the DNA:RNA hybrid, the two-step mechanism uses RNase H instead of B3 primer-initiated strand displacement to release the cDNA. The two mechanisms converge after the formation of first-strand cDNA that is looped on one side. Figure truncated; details of cycling amplification including the loop primers' annealing not shown. Inset shows designated primers—B2 and B2c, B3 and B3c, F1 and F1c are complementary sequences, respectively. Reprinted with permission from reference 42. Copyright 2013 American Chemical Society.

4.4 Mismatches between certain primers and templates reduces efficiency

The developed two-step digital RT-LAMP protocol was tested against four patient samples to evaluate the influence of sequence variation to the efficiency of digital RT-LAMP. As shown in Figure 12, the digital RT-LAMP efficiency were 43% ± 9%, 139% ± 33%, 37% ± 20%, and 0.9% ± 0.2% compared to digital RT-PCR with LTR primers for patient sample #1-4. Sequencing results showed that there were 3, 2, 5 and 5 point mutations in the priming regions of sample #1-4, respectively. Therefore, we concluded that the efficiency of digital RT-LAMP is sensitive to mutations in the priming region of the RNA sequence. The efficiency was dramatically increased (the rightmost column compared to the column that is second from the right) from 0.9% ± 0.2% to 22% ± 1 % when mutations in the critical priming position (such as 3' or BIP primer) were corrected. The high specificity of the LAMP reaction often results in relatively low tolerance to mutations and therefore it would be valuable for the assay to maintain both high specificity and good tolerance to mutations. To achieve this goal, more than one set of primers could be included in a single assay to ensure a higher probability of accurate readings, although this idea needs to be tested experimentally.

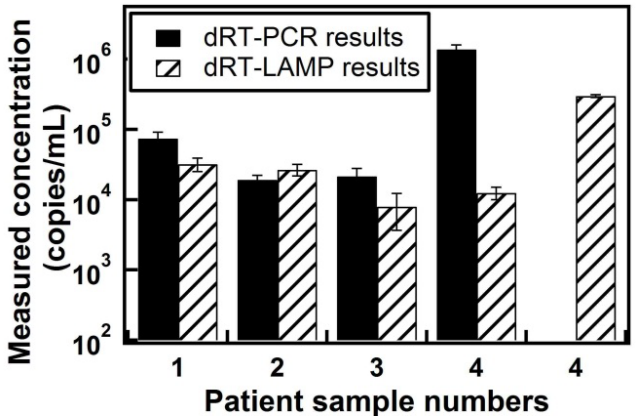

Figure 12 Quantification results of patient HIV RNA samples with digital RT-LAMP and digital RT-PCR. Rightmost column represents the quantification results for sample #4 after primers correction for mutations. Error bars represent standard deviation (n=3). Reprinted with permission from reference 42. Copyright 2013 American Chemical Society.

Single-molecule counting using digital LAMP and digital RT-LAMP is attractive because it is isothermal and does not require thermocycling equipment, and it also provides a bright signal

from the calcein detection system that should be readable by a cell phone. We explored the possibility of using digital RT-LAMP in the quantification of HIV viral load and proposed and tested a two-step protocol for improving the efficiency of this assay. We want to bring to researchers' attention that digital amplification technologies should not always be assumed to provide absolute quantification until validated against a standard.

We have developed new features of the SlipChip microfluidic platform that enable the manipulation of liquid in multiple steps. It not only provide advantages for studying complicated systems, where each step can be isolated and analyzed separately, but also offers possibilities for performing multistep reactions on single targets that need to be isolated, such as single cells. This project also opens the door for performing HIV viral load quantification using isothermal chemistry and simple microfluidic platforms.

CHAPTER 5

FROM THERMAL CYCLING TO ISOTHERMAL: CHALLENGES FOR ROBUSTNESS

5.1 Digital format offers higher robustness than bulk kinetic measurements

Robustness, defined as the consistency of measurement results in the presence of perturbation, is a key factor to consider when designing a POC test. In laboratory settings, robustness is less of a problem because of the availability of dedicated equipment to control experimental conditions precisely. However, such control of reaction conditions often cannot be easily achieved in limited-resource settings, where POC tests are most frequently used. For nucleic acid quantification, nonlinear chemical amplification such as qPCR is usually employed. However, the robustness of such a reaction scheme is not yet fully understood. When quantification is based on the kinetics of an assay, robustness becomes an especially relevant issue, because once the rate of reaction changes, the results of the assay will be influenced directly. While a 3 fold change in HIV viral load could result in a different clinical decision, a change in temperature of a few degrees could potentially shift the results by more than that, as shown below.

We hypothesized that if an end-point digital format instead of real-time kinetic monitoring is used in combination with such exponential amplification, the quantification result will be more robust to potential perturbations, because in a digital format, only identifying yes/no for each compartment is needed for quantification[41a] (Figure 13). In a typical digital analysis, each compartment contains on average less than one molecule, and only those compartments containing target molecules will initiate an amplification reaction and produce a “positive” signal. Therefore, as long as a “positive” or “negative” signal can be identified, knowledge of reaction progress is not required. However, it should be noted that if the initiation of the amplification reaction is influenced by perturbation, the robustness of the digital format needs to be reevaluated.

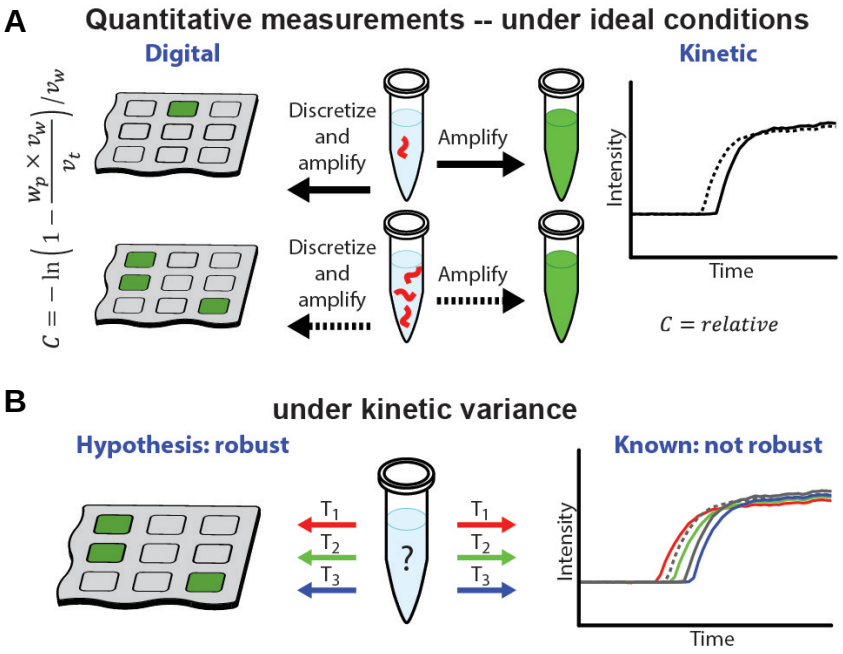

Figure 13 Schematic drawing for the comparison of quantification robustness between digital format and bulk kinetic formats. (A) Quantification of the concentration of the target molecule under ideal conditions: the difference in concentration of the target molecule is reflected by the positive counts in the digital format and the reaction progress in the kinetic measurement. (B) Quantification under non-ideal conditions: the variation in reaction rate does not change the counts in digital format, but influences the reaction progress in the kinetic measurement. Reprinted with permission from reference 41a. Copyright 2013 American Chemical Society.

5.2 Comparison of the robustness between digital quantitative assays and bulk kinetic assays to temperature variation

To evaluate and compare the robustness of digital and kinetic measurements, we used RT-LAMP with an HIV RNA template as a model system. As a rapid, sensitive, and specific isothermal amplification chemistry, RT-LAMP is a good candidate for a POC test, and it has been previously demonstrated on SlipChip microfluidic device for the quantification of HIV viral RNA[42].

We first tested whether quantitative measurements using real-time RT-LAMP assay are robust to temperature fluctuations. Using the two-step protocol developed previously[42] we performed real-time RT-LAMP on an Eco real-time PCR machine. A two-fold change in HIV RNA concentration (1 x 10^5 copies/mL and 2 x 10^5 copies/mL) was successfully distinguished at each

temperature (at 57 °C p = 0.007, at 60 °C p = 0.01, at 63 °C p = 0.04). However, the change in reaction time caused by temperature shifts for each concentration was greater than the change caused by concentration difference (Figure 14A); therefore the two concentrations became indistinguishable if data for different temperatures were grouped together (p=0.25).

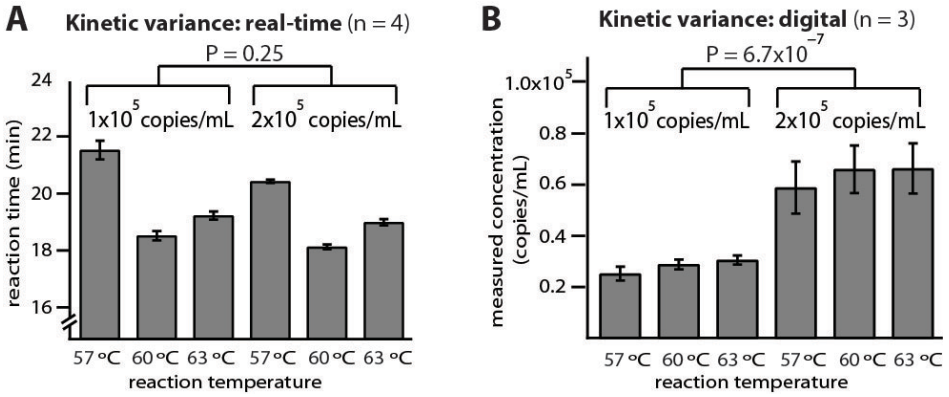

Figure 14 Evaluation of the robustness of real-time RT-LAMP and digital RT-LAMP to variation in temperature. Two concentrations were quantified with A) real-time RT-LAMP and B) digital RT-LAMP assays across a six degree temperature range (n=3). Reprinted with permission from reference 41a. Copyright 2013 American Chemical Society.

The robustness of the digital format of the same RT-LAMP assay was also tested across the same temperature range with the same two concentrations of HIV RNA. The concentration of RNA was determined using Poisson statistics based on the number of positive wells after amplification. Unlike the real-time bulk RT-LAMP assay, the digital RT-LAMP assay could not only distinguish between the two concentrations at each temperature; it could also differentiate the two concentrations despite temperature fluctuations ($p=6.7\times10^{-7}$). We then concluded that the digital RT-LAMP assay for the quantification of HIV RNA is more robust to temperature fluctuation than the real-time RT-LAMP assay.

The lack of robustness of the real-time bulk assay and the robustness of the digital RT-LAMP assay to temperature variation indicated that the amplification rate was influenced significantly, but the probability of reaction initiation was not influenced much by temperature perturbation.

The equilibria of DNA-enzyme, RNA-enzyme, DNA:DNA hybridization, the rate of enzyme attachment and nucleic acid annealing were all temperature-dependent. But again, because the digital format quantification was influenced only by the probability of initiation, it should be more robust to these changes compared with the bulk kinetic assay.

5.3 Comparison of the robustness to changes in assay time for the digital quantitative assay and bulk kinetic assay

Quantification in a digital format is related to the "end-point" of the assay. Ideally, the window for readout should include the minimum number of false negatives (reaction of a single molecule that has not gone to completion) and the minimum number of false positives (non-specific amplification that proceeds at a slower rate), which means the cut-off time should be after all specific amplification turns positive and before non-specific amplification turns positive, and the digital counts should remain stable. To determine the end-point and test whether quantification results of the digital assay were sensitive to this time, we performed a real-time digital RT-LAMP assay with HIV RNA template by imaging the device periodically. Most of the counts turned positive between 20 to 40 minutes, and the change of counts after 40 minutes and before 60 minutes (when false positives started to appear) was less than 10%. A two-fold difference in concentration could be distinguished without any difficulty (Figure 15) regardless of when the reaction was terminated within this 20-minute period.

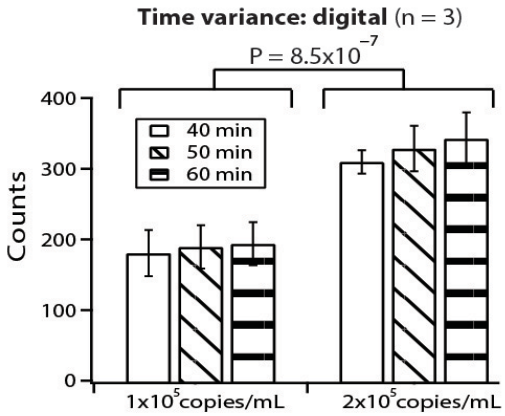

Figure 15 Evaluation of the robustness of digital RT-LAMP to variations in assay time. Two concentrations were quantified with digital RT-LAMP assays and the counts were recorded in a real-time format. Counts at 40, 50 and 60 minutes were plotted (n=3). Reprinted with permission from reference 41a. Copyright 2013 American Chemical Society.

5.4 The integration of digital quantification with cell phone imaging enables direct result readout and feedback

To further evaluate the potential of using digital RT-LAMP for diagnostics in limited-resource settings, we explored the possibility of combining RT-LAMP chemistry with cell phone imaging. We imaged the SlipChip device with the digital pattern after the RT-LAMP reaction with a Nokia 808 Pureview cell phone, which features a 41-megapixel sensor with a pixel size of 1.4 μm. Next, we used a centralized computer with a customized Labview program to process the images, which were automatically uploaded to the server via cloud technology once they were generated (Figure 16). The processed result would then be sent back to the user or doctor for instant feedback. The quantification results of cell phone imaging and data processing were validated against the results obtained by microscope imaging and processed by commercial software.

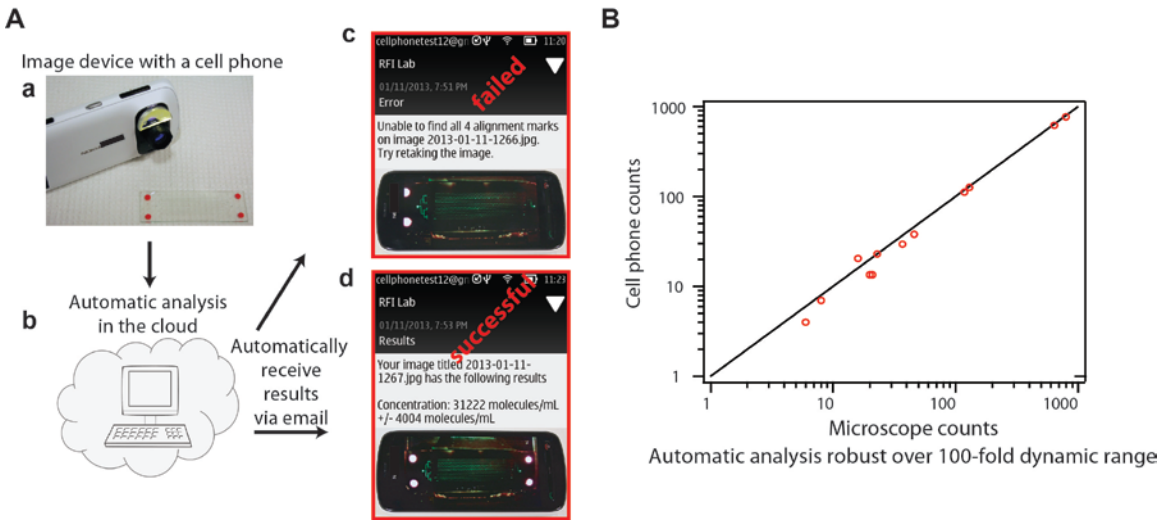

Figure 16 Automatic data analysis workflow and its validation using microscope imaging and Metamorph analysis. A) The image acquisition and analysis workflow with a cell phone and remote server. a)-d): Image was captured by a Nokia phone and transferred via the "cloud" to a remote centralized computer, where software recognized the device and converted the counts into concentration or did not recognize the device and asked the user to retake image. B) Validation of cell phone imaging and analysis with customized Labview program against microscope imaging and analysis with commercial software. Reprinted with permission from reference 41a. Copyright 2013 American Chemical Society.

We understand that the establishment of robust automated counting of HIV RNA molecules using digital amplification chemistry and a cell phone is only part of the full diagnostic assay and several additional advances are needed for it to be used under limited-resource settings, including the integration of a sample preparation module, a simple heating mechanism, and evaluation of robustness to other factors. If all of these elements are addressed, we may see an emergence of rapid amplification schemes that are especially suitable for quantitative measurements under limited-resource settings because of specificity, sensitivity, and robustness.

CHAPTER 6

A SIMPLE METHODOLOGY FOR HCV GENOTYPING AND RELATED INSIGHTS INTO "FATE" AND "RATE" AT THE SINGLE-MOLECULE LEVEL

6.1 The need for simple and easy HCV genotyping assay in limited-resource settings and an overview of existing technologies

HCV is a major public health concern and a leading cause of chronic liver disease and cirrhosis. An estimated population of 180 million are infected with HCV worldwide, and more than 350,000 people die every year from HCV-related liver diseases[45]. There is currently no vaccine for hepatitis C; however, it can be cured using antiviral medicines. Different genotypes respond differently to the same treatment; therefore, determining genotypes or even subtypes before treatment is necessary to adjust the dose and duration of the therapy, and predict the likely outcome. 7 genotypes of HCV are categorized, based on sequence similarity. Genotypes differ from one another by 31-33% at the nucleotide level. The diversity of sequence is not uniform in all regions of the HCV genome—some regions, such as 5'UTR, are quite conserved while other regions, such as E2, are hypervariable. Genotyping is necessary not only for the current standard therapy with PEG-interferon and ribavirin[46], but also for the new small-molecule antiviral drugs such as Sofosbuvir (Gilead)[47].

There are several HCV genotyping assays commercially available including sequencing analysis, real-time Taqman RT-PCR assays, and hybridization-based assays. Sequencing and phylogenetic analysis, such as Siemens TRUGENE HCV Genotype Test, give very accurate sequence information. However, performing sequencing is always time consuming, labor intensive and relatively expensive. Real-time Taqman RT-PCR assays, such as the Abbott RealTime HCV Genotype II assay, require only one RT-PCR step with fluorescent-labeled probes, but face the disadvantages of high initial setup cost and required instrument for real-time monitoring.

Hybridization-based assays, such as Siemens VERSANT HCV Genotype 2.0 assay (LiPA), are the most widely used HCV genotyping method. While they provides more subtype information than real-time PCR Taqman assay, the requirement for stringent control of conditions, a non-negligible degree of error due to secondary structures of the product, and different tolerance to single-nucleotide polymorphisms decrease their robustness. As pointed out, none of the methods discussed above are easily adoptable in limited-resource settings with a simple setup.

6.2 A novel way to use competition—the combination of RT-LAMP and restriction endonuclease to generate sequence-specific signal

Herein we introduced a new method for HCV genotyping based on the combination of isothermal amplification and sequence-specific inhibition. RT-LAMP was selected as the amplification chemistry because of its high tolerance to biological samples and compatibility with simple imaging devices[41a]. Restriction enzymes were chosen as the inhibitor considering their high specificity to DNA sequences under isothermal conditions. The underlying principle is that the inhibition takes place during amplification and the result of amplification itself serves as the readout.

We first retrieved 1398 sequences of HCV RNA from Los Alamos National Lab. All sequences were aligned using Genious software and the consensus of 5'UTR for each genotype was extracted based on the alignment result. RT-LAMP primers targeting 5'UTR were chosen from previous publication[48] and optimized to adapt to all genotypes. Based on the consensus, three restriction endonucleases were chosen to target the sequence differences between these four genotypes within the RT-LAMP amplicon. NheI (targeting GCTAGC) should recognize genotypes 1, 2, and 4; BsrBI (targeting CCGCTC) should recognize genotypes 1, 3, and 4; and BstNI (targeting CCWGG) should recognize only GT1 (Figure 17). Because one restriction endonuclease can probe multiple genotypes, in principle, an unambiguous genotyping panel can

be designed with fewer reactions than genotypes (e.g., three restriction endonucleases to differentiate four genotypes here).

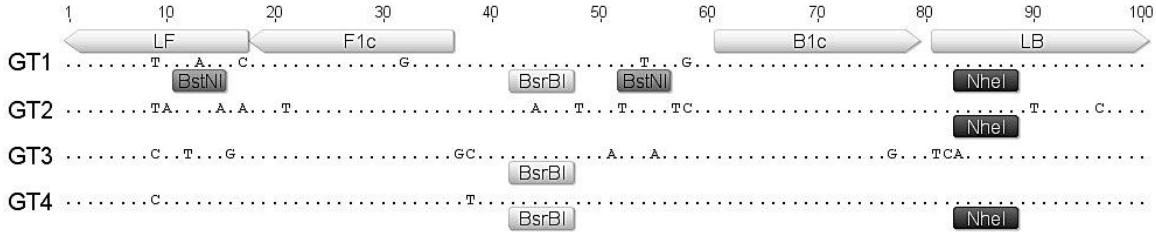

Figure 17 Sequence alignment of the consensus of four genotypes, shown together with the digestion sites of NheI, BsrBI, and BstNI. Dots stand for nucleotides that are the same between genotypes and the SNPs are shown with corresponding letters. LOOP_F (LF), F1c, B1c and LOOP_B (LB) are the priming regions. GT: genotype.

We first performed a real-time bulk measurement of different combinations of genotypes and restriction endonucleases. We obtained HCV isolates of genotypes 1, 2, 3, and 4 from commercial sources and sequenced the purified RNA to confirm the genotype assignment. For each genotype, we performed four experiments: one positive control without restriction endonuclease, and three experiments with one restriction endonuclease each. The experimental results (Figure 18B) agreed with the inhibition pattern predicted (Figure 18A): amplification of GT1 was inhibited by all three restriction endonucleases; amplification of GT2 was inhibited by NheI only; amplification of GT3 was inhibited by BsrBI; and amplification of GT4 was inhibited by NheI and BsrBI. Reactions with restriction endonucleases specific to the genotype were all delayed by a certain amount of time, although not fully inhibited. We then wished to further explore the reason for this delay: does the addition of the restriction enzyme simply slow down the reaction for each molecule, or does it decrease the number of molecules amplified?

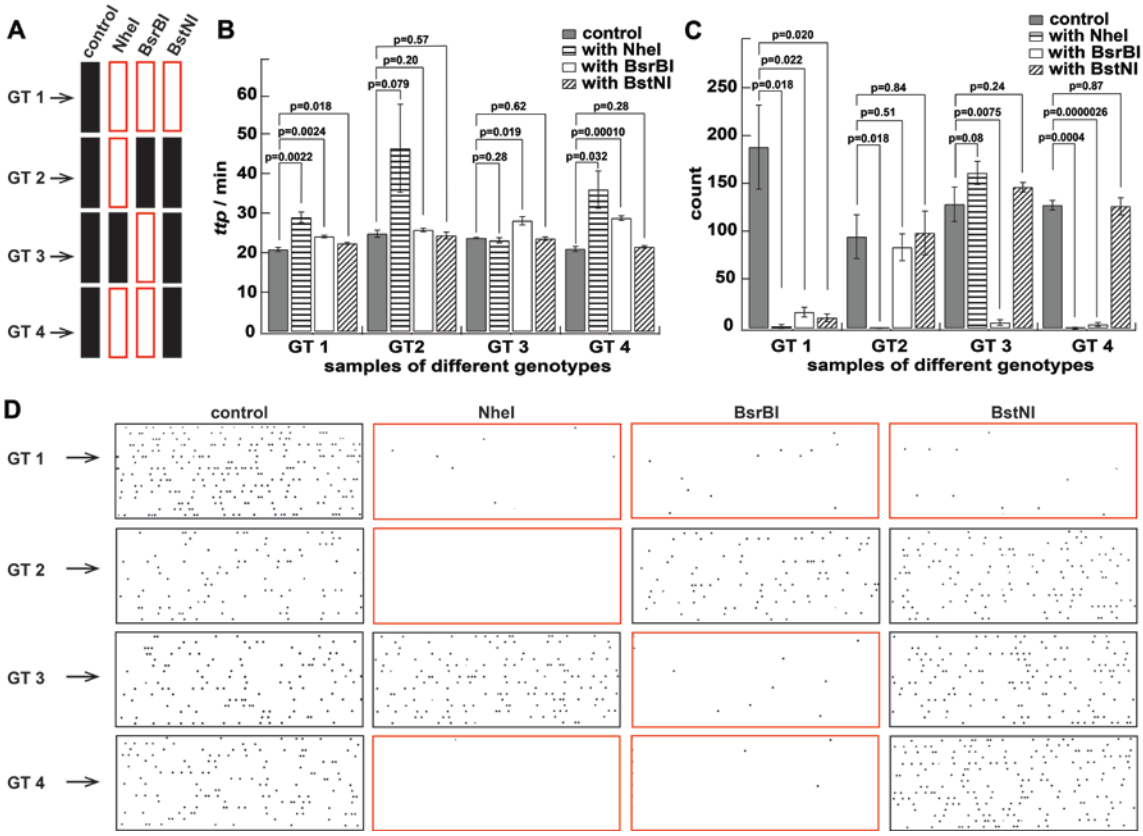

Figure 18 Predicted and experimental HCV genotyping pattern. (A) Prediction matrix for different combination of genotypes and restriction endonucleases. Red indicates predicted inhibition, black stands for normal amplification, and white stands for inhibition. (B) and (C) Graphs showing a comparison of HCV genotyping results using (B) real-time bulk assay (ttp: time-to-positive) and (C) end-point digital assay (n=3). (D) Photographs (inverted intensity) of end-point digital experimental genotyping results. The first column in both sections represents the positive control in the absence of restriction endonuclease and the following three columns indicate experiments with different restriction endonucleases. Each row represents a genotype of HCV RNA. Reproduced from the accepted version of reference 49. Copyright © 2014 WILEY-VCH Verlag GmbH & Co. KGaA

6.3 Improving assay performance when switching to a digital format

One way to answer the question above is to perform the assay in a digital format. We hypothesized that the count in digital format should be a direct measure of the amount of amplified molecules. In the digital format (Figure 18C and D), reactions with restriction endonuclease specific to the genotype showed reduced counts by at least 10 fold with a maximum p-value of 0.022 for all the combinations, indicating that the number of amplified molecules decreased by about 10 fold. Compared to a 10-100% change in bulk time-to-positive, this 10 fold

change significantly improved assay sensitivity. The activity and specificity of restriction endonuclease under LAMP conditions was further confirmed by DNA gel electrophoresis analysis of the digestion product. All four genotypes of HCV RNA were amplified with RT-LAMP before subjected to digestion with NheI-HF, BsrBI, and BstNI at RT-LAMP conditions (63 °C in LAMP buffer). The restriction pattern (Figure 19) matched the one predicted by informatics analysis.

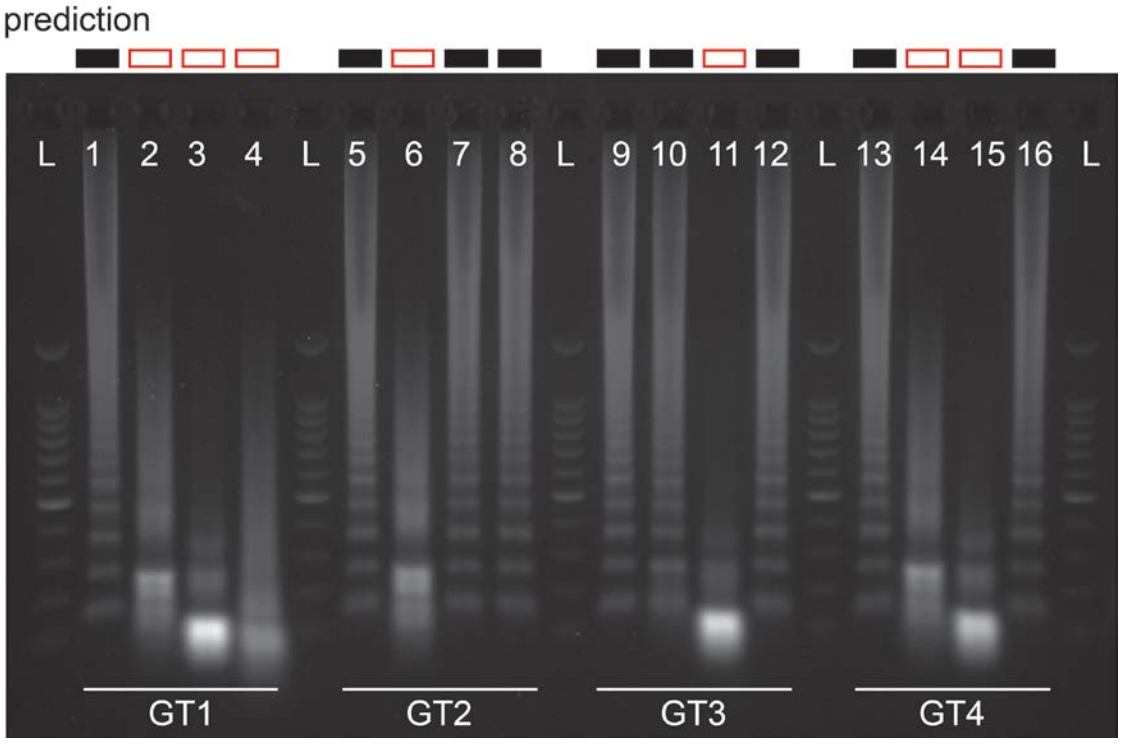

Figure 19 Image of DNA gel electrophoresis results for digestion of RT-LAMP product at RT-LAMP conditions. Lanes labeled with L are 100 bp DNA ladders. Lanes 1-4 are positive control, NheI digestion product, BsrBI digestion product, and BstNI digestion product for genotype 1, respectively. Lanes 5-8 are positive control and 3 RE digestion products for genotype 2. Lanes 9-12 are for genotype 3 and Lanes 13-16 for genotype 4. The specificity of RE to different genotypes are the same as predicted: for genotype 1 all 3 REs digested the product; for genotype 2 only NheI digested the product; for genotype 3 only BsrBI digested the product, and for genotype 4 both NheI and BsrBI digested the product. Reproduced from the accepted version of reference 49. Copyright © 2014 WILEY-VCH Verlag GmbH & Co. KGaA.

Both of these simplified measurements could in principle be used to derive genotype information from the competition between amplification and digestion. The advantage of the real-time

methodology is that it is well-established and the instrument already exists in many research labs. We, however, prefer the end-point digital format for limited-resource settings: it does not require complex instrumentation for performing kinetic measurements; it is expected to be robust to fluctuation in conditions; and it can be read-out with a cell phone, as stated in the published paper[49]. The viral load can be directly read from the positive control as well, giving more information for making clinical decisions. However, we do want to point out that the absolute measurement is not a necessity, because only the "extent" to which the digital counts decrease needs to be measured. The effectiveness of the inhibition chemistry determines the resolution of the digital measurement, with stronger inhibition resulting in lower requirements for resolution.

6.4 The capability of digital to decouple "fate" from "rate" by generating 2D data

To facilitate the discussion, here we use the same definition as in the published paper[49]: "rate" as how quickly amplification proceeds from a single molecule to produce a particular level of a signal and "fate" as whether or not amplification ultimately succeeds to provide that level of signal from a single molecule (Figure 20A). In the actual reaction scheme (Figure 20B), the fate-determining step occurs once the first double-stranded DNA (dsDNA) is formed (structure (1) in Figure 20B): either restriction endonuclease cleaves it, or it escapes the digestion and leads to the formation of the double-looped template that can be further amplified. Net rate of the overall reaction is determined by the rate of amplification and the rate of digestion, and should be the difference between the two.

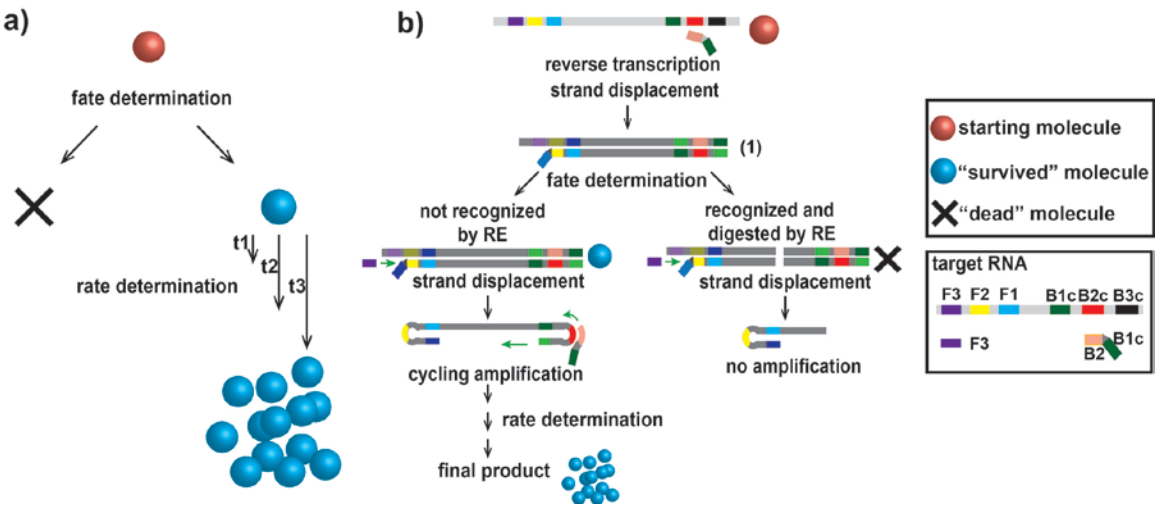

Figure 20 Schematic overview of the definition of "fate" and "rate". (A) In general, "fate" determines whether a molecule can proceed to the final stage of a reaction and "rate" determines how quickly the accumulation of products amplified from one "survived" molecule is. (B) For the competition between RT-LAMP and restriction digestion, "fate" determines whether the first dsDNA gets digested or proceeds to the cycling amplification and "rate" determines how quickly the amplicons accumulate. Reproduced from the accepted version of reference 49. Copyright © 2014 WILEY-VCH Verlag GmbH & Co. KGaA

To validate the hypothesis above, we performed real-time digital RT-LAMP/restriction endonuclease experiments with HCV genotype 1 RNA and BsrBI. The digestion site of BsrBI (CCGCTC) exists in the amplicon of GT1 RNA and therefore should inhibit the amplification. We used a SlipChip microfluidic device modified based on previous publication[42] to compartmentalize the reaction mixture and monitored the progress of amplification for each single compartment. We found significant heterogeneity of rate between molecules and a dramatic change in fate and smaller change in rate of target molecules (shift of mean in Figure 21A and B), indicating that in digital RT-LAMP, BsrBI affects fate more than it affects rate. The median of each set of real-time digital data (23 min for reaction without restriction endonuclease and 30 min for reaction with restriction endonuclease) were quite close to the mean shown in Figure 21A and B, indicating that there were not any data outliers that influenced the mean significantly (in other words, the distribution was close to an symmetric distribution) and that mean could be used to describe the distribution of time-to-positive in this case.

As a comparison, we performed the same competition experiments in the bulk real-time format using an RNA concentration equivalent to that of a single molecule in a well. Without BsrBI, the time-to-positive in this bulk experiment was close to that of the first positive molecule in the digital format (approximately 2 min slower) (Figure 21A). Upon addition of BsrBI, the bulk reaction showed increased variance and slowed down to the same extent as that for the first molecule in the digital format (Figure 21C). These data suggest that once exponential amplification of one molecule initiates, this process dominates the reaction mixture and is not affected by the amplification of the molecules that amplify later. The real-time digital format describes not only the fate, but also the rate of each molecule; thus, it provides more information than bulk real-time, which only reflects the rate of the first few amplified molecules, and end-point digital, which only reflects the fate.

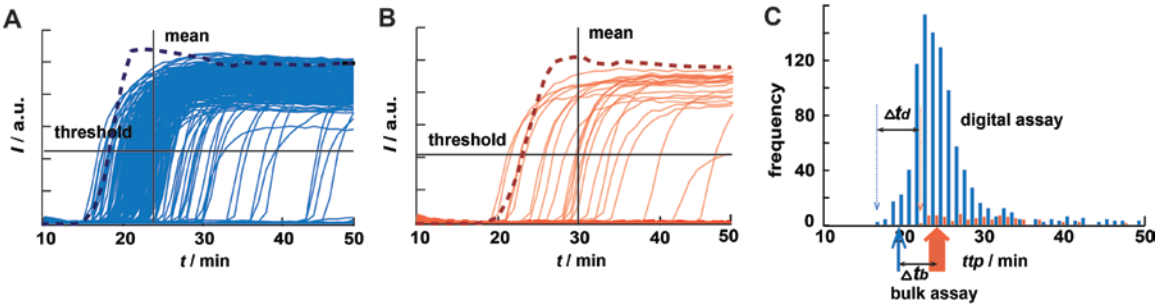

Figure 21 Results of real-time, single-molecule digital RT-LAMP/restriction endonuclease experiments for HCV RNA. (A), (B) Graphs showing 1280 fluorescence traces for the RT-LAMP amplification process of all the wells on a SlipChip device (solid light blue) and averaged fluorescence curve in bulk (dashed dark blue) in the absence of restriction endonuclease (A) and the traces for digital (solid light red) and for bulk (dashed dark red) in the presence of restriction endonuclease BsrBI (B). Horizontal solid lines indicate the threshold levels to consider a well positive. Vertical solid lines show the mean of the time-to-positive distribution. The scales in (A) and (B) are the same. (C) Graph showing the histogram of time-to-positive distribution for wells exceeding the threshold in (A), blue, and (B), red. The two bars below the x-axis show time-to-positive for real-time bulk experiments, the widths of which stand for standard deviation for the bulk assay (n=5). Reproduced from the accepted version of reference 49. Copyright © 2014 WILEY-VCH Verlag GmbH & Co. KGaA

6.5 The connection between single molecule kinetics and bulk kinetics

The next question we asked is how to establish correlation between single molecule kinetics and bulk kinetics based on these findings. As we have discussed previously, bulk kinetics is only determined by the rate of first few amplified molecules. For the sake of simplicity, here we consider the bulk rate as only related to the rate of the first amplified molecule. The effect of various events (adding inhibitors, changing input target concentrations, changing temperatures, etc.) can all be traced to changes in the rate of the first amplified molecule.

In the case of adding restriction endonuclease, the entire distribution is shifted to the right (Figure 22A), which could be captured as the shift of the mean of the distribution from m1 to m2. As a result of this rate change, the first amplified molecule should have a later time-to-positive. Meanwhile, the fate of amplification is changed as well; hence each molecule has a smaller chance of being amplified, presented as the decrease of total counts (area under the peak). As a result, the probability of having molecules amplified at early time points is smaller. The change of time-to-positive from t1 to t2 for the first amplified molecule is a joint effect of both rate change and fate change, and therefore the difference between t1 and t2 (fate and rate effect) should be larger than that between m1 and m2 (pure rate effect). However, if the reaction scheme of amplification changes significantly, which changes the width of distribution, other considerations need to be taken into account to determine the time-to-positive for the first amplified molecule.

The same explanation applies to the case where the amount of input molecules increases (c1 to c2 in Figure 22B). The mean of the distribution will not change because the rate for each molecule is not influenced by the number of total molecules if the reagents are all in excess. The total number of counts and the frequency at each time point, though, will increase. This change of total number of molecules increases the probability of having molecules amplified at an early time point, which shifts the time-to-positive for the first molecule from t1 to t2 (Figure 22B), and causes a bulk time-to-positive decrease. When the concentration goes high enough, increasing number of

input molecules will not further shift the time-to-positive for the first molecule because it has reached the highest possible rate (determined by reaction condition). Further increases in the number of molecules will increase the frequency at this minimum time-to-positive (c2 to c3 in Figure 22B) and cause the bulk time-to-positive to decrease because of higher starting concentration.

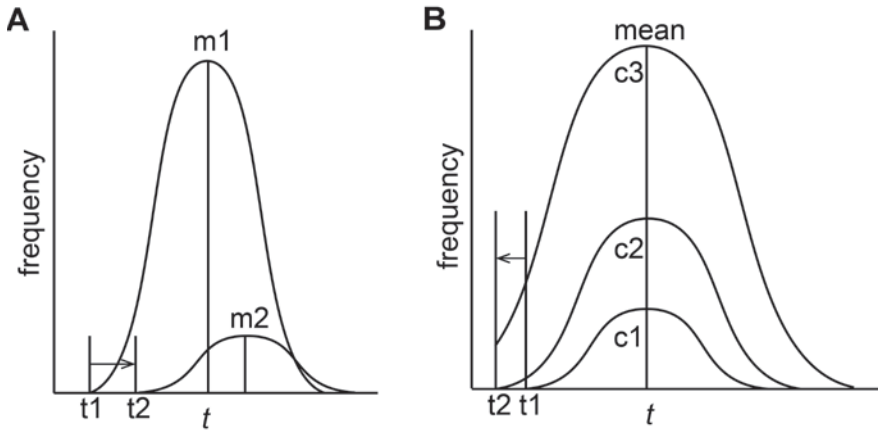

Figure 22 Theoretical histogram of time-to-positive distribution for single molecules (A) in the absence and presence of restriction endonuclease and B) at different input target concentration.

Now we can add some complexity, by discussing when the assumption that the bulk time-to-positive is only related to the first positive molecule holds true. Here a factor to consider is how the reaction progresses from one molecule to the final products in bulk: are all the products generated from one molecule, or from multiple molecules that start to amplify shortly after the first one does. If the amplification from a single molecule is fast enough, in the next minute (or any time frame), it generates more products than the number of molecules that start to amplify; therefore, the amplification in the entire tube is dominated by this one molecule. In this case, the difference between bulk time-to-positive and digital time-to-positive for the first molecule is the difference between time required to generate a positive signal in a 10μL solution in tube and that to generate a signal in a 3nL well. If the amplification from one molecule is slow, in the next minute the number of molecules starting to amplify will exceed the amount of products generated

by that first molecule; therefore the bulk kinetics are determined by multiple molecules starting to amplify at early time points. The difference between bulk time-to-positive and digital time-to-positive for the first molecule is the amount of time required for a certain amount of molecules to start amplification.

More questions raised by the results presented here await to be answered, as stated in the published paper[49]: "What is the right theoretical framework within which to analyze both rate and fate in single-molecule competition reactions? What are the molecular details of the mechanisms responsible for fate and rate determination in such systems? Can robustness of output of these systems be predicted *a priori*? What are the best amplification and inhibition chemistries with which to implement such competition reactions for genotyping and other genetic analyses?"

6.6 Improving the assay coverage by employing another amplification chemistry

The LAMP reaction is performed at 60 °C-65 °C, which is higher than the optimal temperature for many restriction endonucleases. This reduces the number of restriction endonuclease candidates and limits the application of the methodology. In place of LAMP, other isothermal amplification methods performed at lower temperatures have been tested including RPA and NASBA. While restriction endonuclease did not preserve their activity in RPA conditions, specific and complete inhibition of NASBA amplification with restriction endonuclease has been tested to be successful (Table 1). Experimental results agreed well with predicted results for the enzymes tested. Expanding the number of restriction endonuclease grants higher coverage of typable sequences and reduces mistyped and untypable cases. Based on the sequence analysis of 1300 sequences downloaded from Los Alamos National Laboratory, by using a combination of 7 restriction endonuclease, 97.6% of the sequences belonging to genotype 1a, 1b, 2, 3a and 4 can be correctly genotyped, 2% of the sequence are untypable, and only 0.4% of the sequences are mistyped. Moreover, in the RT-LAMP system, *ab initio* synthesis of DNA by Bst DNA

polymerase in the presence of restriction endonuclease limits the amount of restriction endonuclease in the system, which could be the reason for incomplete inhibition in the bulk format. In the NASBA system, no obvious *ab initio* synthesis has been observed; therefore the amount of restriction endonuclease could be increased for better inhibition. A complete stop of the amplification reaction in the bulk format avoids the requirement for real-time monitoring, enabling direct end-point readout for bulk format.

Table 1 Predicted and experimental NASBA results for combinations of genotypes and restriction endonuclease

	NheI	BsrBI	ApoI	BsrGI	BseYI	BstXI	NruI
				Predicted results			
GT 1	–	–	+	+	+	+	–
GT 2	–	+	+	+	–	–	+
	–	+	+	+	+	+	+
	+	+	+	+	–	–	+
	+	+	+	+	+	+	+
GT 3	+	–	–	+	–	+/–*	+/–
GT 4	–	–	+	–	+	+	+/–
	–	–	–	+	+	+	+/–
	–	–	–	–	+	+	+/–
				Experimental results			
GT 1	–	–	+	+			
GT 2	n.t.**	+	+	+		n.t.	
GT 3	+	–	–	+			
GT 4	–	–	n.t.	n.t.			

* +/–: NASBA reaction could be positive or negative. Information extracted from this combination does not contribute to genotyping.
** n.t.: not tested

This research opens the door for sequence-specific recognition using competition reactions. Similar principles could be applied with other sequence-specific inhibitors such as peptide nucleic acid (PNA) and clustered regularly interspaced short palindromic repeats (CRISPR)/Cas9 genome editing systems, other isothermal amplification chemistries, and in any applications such as rare allele detection and cancer diagnosis.

CHAPTER 7

CONCLUDING OVERVIEW

In the work presented here, microfluidics has been used as an important tool to study reactions at the single-molecule level. It does not only provide an alternative approach for quantification via compartmentalization, but also has the capability to decouple different stages and facets of one reaction, which facilitates the study of reaction mechanisms. This is usually difficult for or beyond the capability of other technologies.

Microfluidics provides possibilities for performing molecular diagnosis in limited-resource settings. The confinement of single molecules converts analog signals to digital signals. Such conversion allows the readout to be carried out only at the endpoint of the reaction, rather than real-time monitoring of the entire reaction progress[16]. Furthermore, by confining molecules into different volumes in the same assay and incorporating mathematical considerations, the dynamic range can be enlarged to satisfy the requirements of viral load quantification[32]. In addition, isothermal amplification chemistry could be employed to eliminate the requirement of thermal cycling[35]. All the advances discussed above enable SlipChip microfluidics devices to be used in limited-resource settings for the detection and quantification in diagnostic assays.

The two most important characteristics of such a digital assay—efficiency and robustness—have been studied and a novel concept has been proposed to describe the progress of some reactions. When a reaction is observed at the single-molecule level, the probability for each molecule to initiate the reaction (fate) and how fast the reaction proceeds (rate) can be looked at separately, unlike in a bulk format. The decoupling of “fate” and “rate” in a digital format could increase the assay sensitivity, as in the example of HCV genotyping using RT-LAMP and restriction endonuclease. Furthermore, the monitoring of reaction progress for each single molecule can aid

understanding of whether the presence of any perturbation changes the “fate” or “rate” of a reaction.

The understanding of reaction mechanisms at the single-entity level enabled by microfluidics aids the design and development of new assays to solve real-world problems, which has been demonstrated with applications in HIV and HCV viral load quantification and HCV genotyping. It can also potentially address problems not currently solvable by existing technologies: for example, the co-incidence detection of multiple biomarkers, studying the heterogeneity of cells, bacteria, organisms and molecules, and so forth.

As we have stated in a review[8] by our group, the adoption of single-molecule microfluidics in biology and chemistry should also be accompanied by the effort of making these technologies massively distributed, in terms of both cost and ease of operation. The replacement of glass material by low-cost plastic material has been shown in my work[42] and is one of the future directions for microfluidic platforms to be widely used. The integration of many components for a final “sample-in-result-out” assay is also necessary. Most of the work discussed here focused on the amplification chemistry and detection reaction, but other questions, such as how to extract target nucleic acids from raw sample (such as blood, plasma, and swab) and to test their compatibility with downstream reactions, remain to be answered. Once these elements are tested and characterized, microfluidics will provide unique advantages and opportunities for biology and chemistry.

References

1. Peeling, R. W.; Smith, P. G.; Bossuyt, P. M. M., A guide for diagnostic evaluations. *Nat. Rev.Microbiol.* **2010,** *8* (12 Suppl), S2-6.

2. Yager, P.; Domingo, G. J.; Gerdes, J., Point-of-care diagnostics for global health. *Annu. Rev. Biomed. Eng.* **2008,** *10*, 107-144.

3. Mabey, D.; Peeling, R. W.; Ustianowski, A.; Perkins, M. D., Diagnostics for the developing world. *Nat. Rev. Microbiol.* **2004,** *2* (3), 231-240.

4. Gubala, V.; Harris, L. F.; Ricco, A. J.; Tan, M. X.; Williams, D. E., Point of Care Diagnostics: Status and Future. *Anal. Chem.* **2012,** *84* (2), 487-515.

5. Karim, O.; Rao, A.; Emberton, M.; Cochrane, D.; Partridge, M.; Edwards, P.; Walker, I.; Davidson, I., Point-of-care PSA testing: An evaluation of PSAwatch. *Prostate Cancer Prostatic Dis.* **2007,** *10* (3), 270-273.

6. www.cepheid.com, www.idahotech.com, www.twistdx.co.uk

7. (a) Toner, M.; Irimia, D., Blood-on-a-chip. *Annu. Rev. Biomed. Eng.* **2005,** *7*, 77-103; (b) Chin, C. D.; Linder, V.; Sia, S. K., Lab-on-a-chip devices for global health: Past studies and future opportunities. *Lab Chip* **2007,** *7* (1), 41-57.

8. Ismagilov, R. F., Witters,D., Sun, B., Begolo, S., Rodríguez-Manzano, J., Robles, W., Digital Biology and Chemistry. *Lab Chip* **2014**, accepted.

9. Edd, J. F.; Di Carlo, D.; Humphry, K. J.; Koster, S.; Irimia, D.; Weitz, D. A.; Toner, M., Controlled encapsulation of single-cells into monodisperse picolitre drops. *Lab Chip* **2008,** *8* (8), 1262-1264.

10. Hong, J. W.; Studer, V.; Hang, G.; Anderson, W. F.; Quake, S. R., A nanoliter-scale nucleic acid processor with parallel architecture. *Nat. Biotechnol.* **2004,** *22* (4), 435-439.

11. Rissin, D. M.; Kan, C. W.; Campbell, T. G.; Howes, S. C.; Fournier, D. R.; Song, L.; Piech, T.; Patel, P. P.; Chang, L.; Rivnak, A. J.; Ferrell, E. P.; Randall, J. D.; Provuncher, G. K.; Walt, D. R.; Duffy, D. C., Single-molecule enzyme-linked immunosorbent assay detects serum proteins at subfemtomolar concentrations. *Nat. Biotechnol.* **2010,** *28* (6), 595-599.

12. Wheeler, A. R.; Throndset, W. R.; Whelan, R. J.; Leach, A. M.; Zare, R. N.; Liao, Y. H.; Farrell, K.; Manger, I. D.; Daridon, A., Microfluidic device for single-cell analysis. *Anal. Chem.* **2003,** *75* (14), 3581-3586.

13. Du, W.; Li, L.; Nichols, K. P.; Ismagilov, R. F., SlipChip. *Lab Chip* **2009,** *9* (16), 2286-2292.

14. Li, L.; Du, W.; Ismagilov, R. F., Multiparameter Screening on SlipChip Used for Nanoliter Protein Crystallization Combining Free Interface Diffusion and Microbatch Methods. *J. Am. Chem. Soc.* **2010,** *132* (1), 112-119.

15. Liu, W.; Chen, D.; Du, W.; Nichols, K. P.; Ismagilov, R. F., Slip Chip for Immunoassays in Nanoliter Volumes. *Anal. Chem.* **2010,** *82* (8), 3276-3282.

16. Shen, F.; Du, W.; Kreutz, J. E.; Fok, A.; Ismagilov, R. F., Digital PCR on a SlipChip. *Lab Chip* **2010,** *10* (20), 2666-2672.

17. (a) Cheng, C.-M.; Martinez, A. W.; Gong, J.; Mace, C. R.; Phillips, S. T.; Carrilho, E.; Mirica, K. A.; Whitesides, G. M., Paper-Based ELISA. *Angew. Chem., Int. Ed.* **2010,** *49* (28), 4771-4774; (b) Fang, X.; Liu, Y.; Kong, J.; Jiang, X., Loop-Mediated Isothermal Amplification Integrated on Microfluidic Chips for Point-of-Care Quantitative Detection of Pathogens. *Anal. Chem.* **2010,** *82* (7), 3002-3006.

18. Huynh, T.; Sun, B.; Li, L.; Nichols, K. P.; Koyner, J. L.; Ismagilov, R. F., Chemical Analog-to-Digital Signal Conversion Based on Robust Threshold Chemistry and Its Evaluation in the Context of Microfluidics-Based Quantitative Assays. *J. Am. Chem. Soc.* **2013,** *135* (39), 14775-14783.

19. Dharnidharka, V. R.; Kwon, C.; Stevens, G., Serum cystatin C is superior to serum creatinine as a marker of kidney function: a meta-analysis. *Am. J. Kidney. Dis.* **2002,** *40* (2), 221-6.

20. Shlipak, M. G.; Matsushita, K.; Ärnlöv, J.; Inker, L. A.; Katz, R.; Polkinghorne, K. R.; Rothenbacher, D.; Sarnak, M. J.; Astor, B. C.; Coresh, J.; Levey, A. S.; Gansevoort, R. T., Cystatin C versus Creatinine in Determining Risk Based on Kidney Function. *N. Engl. J. Med.* **2013,** *369* (10), 932-943.

21. Spahillari, A.; Parikh, C. R.; Sint, K.; Koyner, J. L.; Patel, U. D.; Edelstein, C. L.; Passik, C. S.; Thiessen-Philbrook, H.; Swaminathan, M.; Shlipak, M. G., Serum Cystatin C– Versus Creatinine-Based Definitions of Acute Kidney Injury Following Cardiac Surgery: A Prospective Cohort Study. *Am. J. Kidney. Dis.* **2012,** *60* (6), 922-929.

22. Ferguson, M. C., Current therapies for chronic hepatitis C. *Pharmacotherapy* **2011,** *31* (1), 92-111.

23. Kreutz, J. E.; Munson, T.; Huynh, T.; Shen, F.; Du, W.; Ismagilov, R. F., Theoretical Design and Analysis of Multivolume Digital Assays with Wide Dynamic Range Validated Experimentally with Microfluidic Digital PCR. *Anal. Chem.* **2011,** *83* (21), 8158-8168.

24. Vogelstein, B.; Kinzler, K. W., Digital PCR. *Proc. Natl. Acad. Sci. U. S. A.* **1999,** *96* (16), 9236-9241.

25. Beer, N. R.; Hindson, B. J.; Wheeler, E. K.; Hall, S. B.; Rose, K. A.; Kennedy, I. M.; Colston, B. W., On-chip, real-time, single-copy polymerase chain reaction in picoliter droplets. *Anal. Chem.* **2007,** *79* (22), 8471-5.

26. Analytical Chemistry (Washington, D., United States)Sundberg, Scott O.; Wittwer, C. T.; Gao, C.; Gale, B. K., Spinning Disk Platform for Microfluidic Digital Polymerase Chain Reaction. *Anal. Chem.* **2010,** *82* (4), 1546-1550.

27. http://www.lifetechnologies.com/us/en/home/life-science/pcr/real-time-pcr/real-time-openarray.html

28. Shen, F.; Sun, B.; Kreutz, J. E.; Davydova, E. K.; Du, W.; Reddy, P. L.; Joseph, L. J.; Ismagilov, R. F., Multiplexed Quantification of Nucleic Acids with Large Dynamic Range Using Multivolume Digital RT-PCR on a Rotational SlipChip Tested with HIV and Hepatitis C Viral Load. *J. Am. Chem. Soc.* **2011,** *133* (44), 17705-17712.

29. Pawlotsky, J. M., Use and interpretation of virological tests for hepatitis C. *Hepatology* **2002,** *36* (5), S65-S73.

30. Curtis, K. A.; Rudolph, D. L.; Nejad, I.; Singleton, J.; Beddoe, A.; Weigl, B.; LaBarre, P.; Owen, S. M., Isothermal Amplification Using a Chemical Heating Device for Point-of-Care Detection of HIV-1. *PLoS One* **2012,** *7* (2), e31432.

31. Compton, J., NUCLEIC-ACID SEQUENCE-BASED AMPLIFICATION. *Nature* **1991,** *350* (6313), 91-92.

32. Wharam, S. D.; Marsh, P.; Lloyd, J. S.; Ray, T. D.; Mock, G. A.; Assenberg, R.; McPhee, J. E.; Brown, P.; Weston, A.; Cardy, D. L. N., Specific detection of DNA and RNA targets using a novel isothermal nucleic acid amplification assay based on the formation of a three-way junction structure. *Nucleic Acids Res.* **2001,** *29* (11), e54.

33. Vincent, M.; Xu, Y.; Kong, H. M., Helicase-dependent isothermal DNA amplification. *EMBO Rep.* **2004,** *5* (8), 795-800.

34. Notomi, T.; Okayama, H.; Masubuchi, H.; Yonekawa, T.; Watanabe, K.; Amino, N.; Hase, T., Loop-mediated isothermal amplification of DNA. *Nucleic Acids Res.* **2000,** *28* (12), e63.

35. Piepenburg, O.; Williams, C. H.; Stemple, D. L.; Armes, N. A., DNA detection using recombination proteins. *PLoS Biol.* **2006,** *4* (7), 1115-1121.

36. Fire, A.; Xu, S. Q., Rolling replication of short DNA circles. *Proc. Natl. Acad. Sci. U. S. A.* **1995,** *92* (10), 4641-4645.

37. Walker, G. T.; Fraiser, M. S.; Schram, J. L.; Little, M. C.; Nadeau, J. G.; Malinowski, D. P., STRAND DISPLACEMENT AMPLIFICATION - AN ISOTHERMAL, INVITRO DNA AMPLIFICATION TECHNIQUE. *Nucleic Acids Res.* **1992,** *20* (7), 1691-1696.

38. Van Ness, J.; Van Ness, L. K.; Galas, D. J., Isothermal reactions for the amplification of oligonucleotides. *Proc. Natl. Acad. Sci. U. S. A.* **2003,** *100* (8), 4504-4509.

39. Ménová, P.; Raindlová, V.; Hocek, M., Scope and Limitations of the Nicking Enzyme Amplification Reaction for the Synthesis of Base-Modified Oligonucleotides and Primers for PCR. *Bioconjugate Chem*. **2013**, 24 (6), 1081-1093..

40. Seelig, G.; Soloveichik, D.; Zhang, D. Y.; Winfree, E., Enzyme-free nucleic acid logic circuits. *Science* **2006,** *314* (5805), 1585-1588.

41. (a) Selck, D. A.; Karymov, M. A.; Sun, B.; Ismagilov, R. F., Increased Robustness of Single-Molecule Counting with Microfluidics, Digital Isothermal Amplification, and a Mobile Phone versus Real-Time Kinetic Measurements. *Anal. Chem.* **2013,** *85* (22), 11129-11136; (b) Goto, M.; Honda, E.; Ogura, A.; Nomoto, A.; Hanaki, K.-I., Colorimetric detection of loop-mediated isothermal amplification reaction by using hydroxy naphthol blue. *Biotechniques* **2009,** *46* (3), 167-172.

42. Sun, B.; Shen, F.; McCalla, S. E.; Kreutz, J. E.; Karymov, M. A.; Ismagilov, R. F., Mechanistic Evaluation of the Pros and Cons of Digital RT-LAMP for HIV-1 Viral Load Quantification on a Microfluidic Device and Improved Efficiency via a Two-Step Digital Protocol. *Anal. Chem.* **2013,** *85* (3), 1540-1546.

43. Gansen, A.; Herrick, A. M.; Dimov, I. K.; Lee, L. P.; Chiu, D. T., Digital LAMP in a sample self-digitization (SD) chip. *Lab Chip* **2012,** *12* (12), 2247-2254.

44. Curtis, K. A.; Rudolph, D. L.; Owen, S. M., Rapid detection of HIV-1 by reverse-transcription, loop-mediated isothermal amplification (RT-LAMP). *J. Virol. Methods* **2008,** *151* (2), 264-270.

45. Ghany, M. G.; Strader, D. B.; Thomas, D. L.; Seeff, L. B., Diagnosis, Management, and Treatment of Hepatitis C: An Update. *Hepatology* **2009,** *49* (4), 1335-1374.

46. Hnatyszyn, H. J., Chronic hepatitis C and genotyping: the clinical significance of determining HCV genotypes. *Antivir. Ther.* **2005,** *10* (1), 1-11.

47. Hsu, C.-S., Sofosbuvir for Previously Untreated Chronic Hepatitis C Infection. *N. Engl. J. Med.* **2013,** *369* (7), 678-678.

48. Kargar, M.; Askari, A.; Doosti, A.; Ghorbani-Dalini, S., Loop-Mediated Isothermal Amplification Assay for Rapid Detection of Hepatitis C virus. *Indian J. Virol.* **2012,** *23* (1), 18-23.

49. Sun, B., Rodriguez-Manzano, J., Selck, D. A., Khorosheva, E., Karymov, M. A., and Ismagilov, R. F., Measuring Fate and Rate of Single-Molecule Competition of Amplification and Restriction Digestion, and Its Use for Rapid Genotyping Tested with Hepatitis C Viral RNA. *Angew. Chem., Int. Ed.* **2014**, accepted.

APPENDIX A

Authorship contribution statement and experimental section for Chapter 2

In the following publication[18]

Huynh, T.; Sun, B.; Li, L.; Nichols, K. P.; Koyner, J. L.; Ismagilov, R. F., Chemical Analog-to-Digital Signal Conversion Based on Robust Threshold Chemistry and Its Evaluation in the Context of Microfluidics-Based Quantitative Assays. *J. Am. Chem. Soc.* **2013,** *135* (39), 14775-14783.

T.H. and R.F.I. designed the SlipChip experiments.

T.H. was the lead researcher for all figures (Figure 2 and Figure 3 in this dissertation) except for Figure 3 (Figure 4 in this dissertation).

B.S. performed the experiments for Figure 3 (Figure 4 in this dissertation) and helped with FEP coating of the device.

L.L. helped on chip design with the washing channel

K.P.N helped with device surface coating.

J.L.K provided patient samples.

T.H. and R.F.I. wrote the paper.

Experimental section (as described in the publication above)

Chemicals and materials

Phosphate buffer (PB) was a solution of sodium phosphate 0.1 M, pH 7 with Pluronic F127 Prill (BASF) 1 mg/mL. This buffer was made from NaH_2PO_4 (Fisher BP329) and Na_2HPO_4 (Fisher BP332). BAB was a solution of pluronic F127 1 mg/mL in 1xDPBS (10x Gibco 14200 2/2010) pH 7. Starch solution was the suspension of cornmeal in phosphate buffer heated in a boiling water bath for 10 minutes and cooled down to room temperature. The supernatant was then filtered through a syringe filter with a 5-µm membrane to give the starch solution. Inhibitor was a gift by Roman Manetsch and Jordany Maignan (University of South Florida). It was dissolved in DMSO (Fisher D128) to make a 1 mM solution, which was diluted in PB into lower concentrations. Substrate is a mixture of 98 µL starch solution, 1 µL acetylthiocholine (AcSCh) (Sigma A5626) solution (0.4 M in PB), and 1 µL of the 4.016 mL solution of NaI (798.07 mg) (Fisher S324) and I_2 (101.93 M) (Fisher I37) in PB were vortexed in a 600-µL microcentrifuge tube. The substrate mixture was made freshly for each assay. Antibody mixture was 0.709 µL bead-antibody (141 mg/mL), 0.500 µL antibody-biotin (4 OD/cm), and 18.8 µL BAB mixed by pipetting at the time of the assay. Avidin-AChE solution was 1 µL of avidin-AChE (3.36 OD/cm) mixed with 66.2 µL BAB, and stored at 0–4° C.

Conjugation

Bead-antibody: Cystatin C antibody clone 24 (Genway, cat#20-511-242278) was conjugated to tosylated paramagnetic beads (Invitrogen, cat#65501) following the manufacturer's instructions. The approximated final concentration was 141 mg/mL (beads) in PBS (pH 7 with BSA 0.1%, Tween 20 0.05%, and sodium azide 0.02%). The mass of antibody was approximated at 1/8 the mass of beads.

Antibody-biotin: Cystatin C antibody clone 10 (Genway, cat#20-511-242277) was conjugated to biotin using Lightning Link (Novus Biological, cat#704-0015) following the manufacturer's instructions. The buffer was PB, and the absorbance at 280 nm was 4 OD/cm.

Avidin-acetylcholinesterase (avidin-AChE): acetylcholinesterase (AChE) (SigmaAldrich, cat#C2888) (1000 units, 1210 units/mg protein) was conjugated to avidin using Lightning Link (Novus Biological, cat#717-0015) (1 mg avidin). The buffer was sodium phosphate 25 mM, pH 7.2 with Pluronic F127 1 mg/mL. The absorbance at 280 nm was 3.36 OD/cm

Robustness with respect to temperature and detection time

We checked the working ranges of temperature and reaction time of the threshold chemistry using absorbance readout with 5,5'-dithiobis-(2-nitrobenzoic acid) (DTNB)3 (Sigma-Aldrich D8130) (to react with thiocholine, the product of the enzymatic reaction). In each well in the 96-well plates, acetylcholinesterase (AChE) was incubated with the inhibitor for 30 minutes, followed by the addition of a solution of DNTB and acetylthiocholine (AcSCh) and absorbance measurement at 412 nm by a plate reader (BMG LABTECH, POLARstar Omega). The total volume in each well was 80 µL, and the final concentrations of AcSCh and DTNB were 0.2 mM and 0.15 mM, respectively. The inhibitor concentrations used in each set of experiments were 13, 16, 21, 27, 36, and 46 nM. We also investigated the robustness when the concentrations of the enzyme and the inhibitor were 10 times smaller. The temperatures were 22, 25, 28, 31, and 34 °C.

Threshold chemistry in bulk with visual readout

Solutions of 23 µL of enzyme and inhibitor (in PB) were incubated in the wells of a 96-well plate at room temperature for 30 minutes. Then 20 µL of the substrate mixture was added in each of the wells. The image was taken after 39 minutes of reaction using a stereoscope with incident light. The image was subtracted from an image taken after 151 minutes of reaction, when all wells had reacted (as a background subtraction), and then corrected with Photoshop (contrast+95).

Device (SlipChip) fabrication

The SlipChip was fabricated by wet-etching glass plates coated with chromium and photoresist (Telic, soda lime 0.7 mm thick, positive photoresist) with exposed areas from photolithography (mask printed by CadArt), with a twice-concentrated etching mixture (666 mL water, 30 g NH_4F, 78 mL HNO_3 70%, 56 mL HF mix (SigmaAldrich 01066). To etch features of different depths on the same chips, features with shallower depths were covered with packing tape at the beginning and the tape was later removed to expose the features during the process. The depths of the features measured by a contact profiler (Dektak 150) were 142 μm for the analyte wells of the top plate, 22 μm for the rest of the top plate, and 130 μm for the bottom plate. The inlets (on the top plate) and the alignment holes (on both plates) were formed by drilling the chips using 0.035 in drill bits (Harvey Tool 74335-C4).

Treatment of chip surface

The chips were coated with FEP to prevent wetting of the surface by aqueous solutions in areas that do not contain any features (wells or ducts). The glass chips were cleaned in H2SO4 98% : H_2O_2 30% (3:1 v/v) for 1 hour, then sonicated in NaOH (concentrated, ~ 50 g/L). They were then dip-coated in FEP emulsion (Fuel Cell Earth LLC, cat#TE9568-250) diluted 3 times with Millipore water (advancing and withdrawing speeds of 10.8 and 1.8 cm/min, respectively). The coated chips were baked on a hot plate at 250 °C (30 min total time, including heating up from room temperature and baking at 250 °C) and at 340 °C for 1 minute, then cooled in air at room temperature. The chips were then incubated in deionized water for 2.5 hours, and then dried with a N_2 stream. The features designed to contain aqueous droplets had their FEP layer removed either completely (in the case of the top plate) or partially (in the case of the bottom plate) to ensure retention of the droplets during droplet deposition and transfer during the assay. The FEP layer in wells and washing channels on the bottom plate were partially removed by laser

machining (Resonetics RapidX250 system, with demagnification of 10, constant energy mode of 50 mJ with 50 % attenuator, 75-mm lens, and fluence of 9.32 J/cm^2). The ablated areas were approximately half of those of the features and were centered in the features. The FEP coating of wells on the top plate were removed manually and completely with a needle (27G1/2, Beckton-Dickinson 305109) under deionized water. The process was performed under a stereoscope. Another purpose of the removal of FEP in the analyte wells was so that the analyte solutions would wet and fill the wells completely.

Setting up the assay

The bottom plate was put in a square petri dish (Fisher 08-757-11A) filled with FC-40 (3M). The side with features was facing up, and the plate was separated from the bottom of the petridish by the ends of insect pins inserted into the alignment holes. Washing solutions were deposited into the washing channels by pipetting with volumes of 0.5 µL (BAB), 1.2 µL (BAB), and 0.7 µL (PB), following the progress of the assay. Solutions (1 µL) of inhibitor were deposited into inhibitor wells by pipetting with low-retention pipette tips. Solutions of antibody mixture and substrate mixture were made at the time of the experiment. Plugs were made and deposited onto the bottom piece.4 Plugs were made with a cross channel (Idex Health & Science P-634). FC-40 flowed into two opposite inlets with rate of 80 µL/min each (B-D plastic syringe 1 mL (B-D REF 309602), needle 23G1½, B-D 305194, tubing FEP 1/16x0.20x50ft (Idex Health & Science 1548L)). The aqueous solution flowed into the remaining inlet at 40 µL/min (B-D plastic syringe 1 mL (B-D REF 309602), needle 18G1½, B-D 305196, tubing FEP 1/16x0.20x50ft (Idex Health & Science 1548L)). The syringe for the aqueous inlet was filled with FC-40, then with a small air bubble, then the actual aqueous solution so that the aqueous solution stayed in the FEP tubing only. The pumps used to make plugs were Harvard PHD 2000. Plugs were put into FEP tubing 1/16x0.20x50ft (Idex Health & Science 1548L). The tip of the outlet tubing was cleaned using a piece of Kimwipe (Kimberly-Clark) wetted with D.I. water prior to making each set of plugs.

After the series of plugs were formed in the outlet tubing, the flow rate was slowed down to 20 μL/min during deposition, and to 2 μL/min during the movement to another bottom plate. The sequence of solutions that were deposited was as follows: substrate mixture, avidin-AChE, and antibody mixture. The plug-making apparatus was washed by making plugs of BAB between uses with different solutions. After all the solutions were loaded onto the bottom plate, the top plate was placed onto the bottom plate with its alignment holes going over the insect pins. The chips were then taken out of the petri dish with a pair of tweezers, clamped with plastic clothespins (3 on each of two opposite sides of the chip), and aligned with better accuracy under a stereoscope.

Running the assay

Loading: The sample (10 μL) was loaded into the inlet with a pipette tip.

Incubation: When the analyte wells were completely filled with the sample, they were slipped to overlap with the wells containing the antibody mixture. The magnet (long enough to cover the whole row of wells) was used to pull the beads up to the top plate, then to the bottom plate, for a total of 2–3 iterations of back-and-forth movement in the direction of slipping, and the magnet was pulled away from the chip when it was at the middle of the row. The 6 clothespins were replaced with 2 clamps (plastic clamp grips for paper, cut into pieces that fit the chip) on opposite sides of the chip. The chip was incubated in an inverted position (bottom plate up) in a petri dish containing FC-40 at room temperature for 1 hour.

End of incubation: After the incubation, the chip was taken out of the petri dish and held by hand in the proper position (top plate up). The magnet was used to pull the beads to the top plate. The magnet was then held on the top plate during slipping to move the wells containing the beads in contact with the first washing channel.

Washing: The magnet was used to move the beads through the washing phase. The magnet was then held on the top plate near the beads during slipping to move the beads to the next step. The

beads underwent incubation and washing as described above. Each of the incubations with avidin-AChE and the inhibitor also lasted 1 hour at room temperature with the chip in the inverted position in the petri dish containing FC-40.

Initiation of reaction: After the incubation with the inhibitor, the chips were taken out of the petri dish, held by hand in the proper position. The magnet was used to bring the beads into the dumbbell-shaped wells in the top plate. The magnet was held onto the top plate during slipping to bring the wells that contained the beads into contact with the substrate wells. The magnet was used to move the beads to the direction of slipping, then immediately opposite. This moment was set as 0, the beginning of reaction time. During the reaction, the chip was left in air at room temperature. Images of assay results were taken at 70 minutes after the initiation of the reactions.

Handling of images of assay results

Images taken with a digital SLR camera: We used a Canon RebelXT with EFS18-55mm lens. The images were cropped and processed in Photoshop (selective color: hue 0, saturation -100, lightness +50; brightness -5, contrast +50). Images taken with a camera phone: We used an iPhone4 (Apple Inc.). The images were cropped and processed in Photoshop (brightness +50, contrast +50).

Estimation of threshold concentration from assay results of standards and patient samples

The smallest increase of [cystatin C] that led to a change in the position of ON/OFF transition was 0.64–0.75 mg/L (1.2 fold). Therefore, we estimated the threshold concentration in column 2 as 0.69 = (0.64*0.75)0.5 and used this value to estimate the threshold concentrations in other columns, based on 2-fold steps in inhibitor concentrations.

APPENDIX B

Authorship contribution statement and experimental section for Chapter 3

In the following publication

Shen, F.; Sun, B.; Kreutz, J. E.; Davydova, E. K.; Du, W.; Reddy, P. L.; Joseph, L. J.; Ismagilov, R. F., Multiplexed Quantification of Nucleic Acids with Large Dynamic Range Using Multivolume Digital RT-PCR on a Rotational SlipChip Tested with HIV and Hepatitis C Viral Load. *J. Am. Chem. Soc.* **2011,** *133* (44), 17705-17712.

F.S., B.S., J.E.K., W.D. and R.F.I. designed the SlipChip experiments.

F.S. was involved in design and discussion of all figures and was the lead researcher for Figure 1 (Figure 6A in this dissertation), 2 (Figure 6B in this dissertation), 3, 4, and 6.

B.S. was the lead researcher for Figure 5 (Figure 7 in this dissertation).

F.S. and B.S. performed experiments and J.E.K., F.S., B.S. performed data analysis. E.K.D. prepared control RNA and viral RNA used in the experiments.

F.S., B.S., J.E.K. and R.F.I. wrote the paper.

P.L.R and L.J.J. provided the deidentified patient samples, and performed viral load tests with Roche system in parallel.

P.L.R. and L.J.J. also provided suggestions on HIV viral load protocols.

Experimental section (as described in the publication above)

Chemicals and Materials

All solvents and salts obtained from commercial sources were used as received unless otherwise stated. SsoFast EvaGreen SuperMix (2X) was purchased from Bio-Rad Laboratories (Hercules, CA). One-Step SuperScript® III Reverse Transcriptase, iPrepTM purification instrument, and iPrepTM PureLinkTM virus kit were purchased from Invitrogen Corporation (Carlsbad, CA). All primers were purchased from Integrated DNA Technologies (Coralville, IA). Bovine serum albumin (20 mg/mL) was ordered from Roche Diagnostics (Indianapolis, IN). Mineral oil, tetradecane, and DEPC-treated nuclease-free water were purchased from Fisher Scientific (Hanover Park, IL). Dichlorodimethylsilane was ordered from Sigma-Aldrich (St. Louis, MO). PCR Mastercycler and in situ adapter were purchased from Eppendorf (Hamburg, Germany). Spectrum food color was purchased from August Thomsen Corp (Glen Cove, NY). Soda-lime glass plates coated with layers of chromium and photoresist were ordered from Telic Company (Valencia, CA). Photomasks were designed using AutoCAD (San Rafael, CA) and ordered from CAD/Art Services, Inc. (Bandon, OR). MicropositTM MFTM-CD-26 developer was purchased from Rohm and Hass Electronic Materials LLC (Marlborough, MA). Amorphous diamond coated drill bits were purchased from Harvey Tool (0.030 inch cutter diameter, Rowley, MA). Adhesive PDMS film (0.063 inch thick) was purchased from McMaster (Atlanta, GA). The MinElute PCR purification kit and QIAamp Viral RNA mini kit were purchased from Qiagen Inc. (Valencia, CA). The OptiQuant®-S HCV RNA quantification panel was purchased from AcroMetrix (Benicia, CA).

Fabrication of SlipChip for multivolume digital RT-PCR

The procedure for fabricating the SlipChip from soda lime glass was based on the procedure described in previous work. To fabricate SlipChip for multivolume digital RT-PCR, wells of two

different depths were etched using a two-step exposing-etching protocol. The soda lime glass plate pre-coated with chromium and photoresist was first aligned with a photomask containing the design for part of the wells. The glass plate was then exposed to UV light using standard exposure protocols. After exposure, the glass plate was detached from the photomask and immersed in developer to immediately remove the photoresist that was exposed to UV light. The underlying chromium layer that was exposed was removed by applying a chromium etchant (a solution of 0.6:0.365 mol/L $HClO_4$ / $(NH_4)_2Ce(NO_3)_6$). The glass plate was thoroughly rinsed with water and dried with nitrogen gas. The glass plate was then aligned with a second photomask containing the designs of the rest of the wells. The glass plate was then exposed to UV light a second time. After the second exposure, the photomask was detached from the glass plate, and the back side of the glass plate was protected with PVC sealing tape. The taped glass plate was then immersed in a glass etching solution (1:0.5:0.75 mol/L $HF/NH_4F/HNO_3$) to etch the glass surface where chromium coating was removed in the previous step (areas containing wells of 25 nL, 125 nL, and 625 nL), and the etching depth was measured by a profilometer. After the larger features were etched to a depth of 70 μm, the glass plate was placed in the developer again to remove the previously exposed photoresist in areas containing the patterns for the smaller features. The underlying chromium layer was removed by using the chromium etchant as describe above, and a second glass etching step was performed to etch all features to a further depth of 30 μm. The final SlipChip contained wells of depths of 100 μm and 30 μm was fabricated. After the two-step etching, the glass plate was thoroughly rinsed with Millipore water and ethanol and then dried with nitrogen gas. The glass plate was oxidized using a plasma cleaner and immediately placed in a desicator with dichlorodimethylsilane for gas-phase silanization. After one hour, the silanized glass plate was thoroughly rinsed with chloroform, acetone, and ethanol, and then dried with nitrogen gas. To re-use the glass SlipChips, each SlipChip was thoroughly cleaned with piranha acid (3:1 sulfuric acid: hydrogen peroxide), then oxidized using a plasma cleaner and silanized as described above.

Assembling the SlipChip

The SlipChip was assembled under de-gassed oil (mineral oil: tetradecane 1:4 v/v). The bottom plate was immersed into the oil phase with the patterned wells facing up, and the top plate was then immersed into the oil phase and placed on top of the bottom plate with the patterned side facing down. The two plates were aligned under a stereoscope (Leica, Germany) and stabilized using binder clips.

Loading the SlipChip

A through-hole was drilled in the center of the top plate to serve as the solution inlet. The reagent solution was loaded through the inlet by pipetting. For the multiplexed design, five through-holes were drilled at the top left corner of the top plate to serve as fluid inlets. For multiplex experiments, five different reaction solutions were placed in the inlet reservoirs, and a dead-end filling adapter was placed on top of the SlipChip to cover all the inlets. A pressure of 18 mmHg was applied to load all the solutions simultaneously. The principle and detailed method for dead-end filling are described in a previous work. Reservoirs were removed after the solution was loaded.

Synthesis and purification of control RNA (906nt)

The control RNA (906 nucleotide) was synthesized from the LITMUS 28iMal Control Plasmid using a HiScribe™ T7 In Vitro Transcription Kit with the manufacture's recommended procedures (New England Biolabs, Ipswich, MA) and purified using MinElute PCR purification kit with manufacture recommended protocols.

Automatic Viral RNA purification from plasma sample

Plasma samples containing the HIV virus were obtained from deidentified patients at the University of Chicago Hospital. Plasma containing a modified HCV virus as a control (25 million IU/mL, part of OptiQuant-S HCV Quantification Panel) was purchased from AcroMetrix (Benicia, CA). A plasma sample of 400 μL was mixed with 400 μL lysis buffer (Invitrogen Corporation, Carlsbad, CA) to lyse the virus. Then 2 μL of control RNA (906 nt) was added to characterize the purification efficiency and concentrating factor. The mixed sample was then transferred into the iPrepTM PureLinkTM virus cartridge. The cartridge was placed in the iPrepTM purification instrument and the purification protocol was performed according to the manufacturer's instructions. The final elution volume was 50 μL, therefore a theoretical eight-fold concentrating factor was expected. The initial concentration of control RNA and the concentration of control RNA in the purified sample after preparation were characterized on the SlipChip. The final concentrating factor was 4.5 for HCV and 6.6 for HIV in the multiplex RT-PCR amplification.

Primer sequences for RT-PCR amplification

Primers for the control RNA (906 nt) were: GAA GAG TTG GCG AAA GAT CCA CG and CGA GCT CGA ATT AGT CTG CGC. The control RNA template was serially diluted in 1 mg/mL BSA solution. The RT-PCR mix contained the following: 30 μL of 2 × EvaGreen SuperMix, 1 μL of each primer (10 μmol/L), 3 μL of BSA solution (20 mg/mL), 1.5 μL of SuperScript® III Reverse Transcriptase, 17.5 μL of nuclease-free water, and 6 μL of template solution.

Primer sequences for HIV viral RNA: GRA ACC CAC TGC TTA ASS CTC AA; GAG GGA TCT CTA GNY ACC AGA GT.

Primer sequences for control HCV viral RNA were selected from a previous publication: GAG TAG TGT TGG GTC GCG AA; GTG CAC GGT CTA CGA GAC CTC.

RT-PCR amplification on the SlipChip

To amplify HIV viral RNA, the RT-PCR mix contained the following: 15 μL of 2 × EvaGreen SuperMix, 0.6 μL of each primer (10 μmol/L), 1.5 μL of BSA solution (20 mg/mL), 0.75 μL of SuperScript® III Reverse Transcriptase, 10.05 μL of nuclease-free water, and 1.5 μL of template solution. The template solution used here was diluted 250-fold from the original HIV viral RNA stock solution purified from Patient sample 2 using 1 mg/mL BSA solution.

To amplify control HCV viral RNA, the RT-PCR mix contained the following: 15 μL of 2 × EvaGreen SuperMix, 0.25 μL of each primer (10 μmol/L), 1.5 μL of BSA solution (20 mg/mL), 0.75 μL of SuperScript® III Reverse Transcriptase, 10.25 μL of nuclease-free water, and 2 μL of template solution. The template solution was diluted 5-fold from the original control HCV viral RNA stock solution purified from OptiQuant-S HCV Quantification Panel.

To amplify the control RNA (906 nt) in the HIV sample, the RT-PCR mix contained the following: 20 μL of 2 × EvaGreen SuperMix, 1 μL of each primer (10 μmol/L), 2 μL of BSA solution (20 mg/mL), 1 μL of SuperScript® III Reverse Transcriptase, 13 μL of nuclease-free water, and 2 μL of HIV viral RNA stock solution after sample preparation.

The concentration of control RNA (906 nt) before sample preparation was characterized with the RT-PCR mix contained the following: 20 μL of 2 × EvaGreen SuperMix, 1 μL of each primer (10 μmol/L), 2 μL of BSA solution (20 mg/mL), 1 μL of SuperScript® III Reverse Transcriptase, 13 μL of nuclease-free water, and 2 μL of template solution. The template was prepared by diluting 2 μL of stock control RNA (906nt) solution into 400 μL of 1 mg/mL BSA solution.

The amplifications were performed using a PCR mastercycler machine (Eppendorf). To amplify the RNA, an initial 30 min at 50 °C was applied for reverse transcription, then 2 min at 95 °C for enzyme activation, followed by 35 cycles of 1 min at 95 °C, 30 sec at 55 °C and 45 sec at 72 °C.

After the final cycle, a final elongation step was applied for 5 min at 72 °C. This thermal cycling program was applied to all experiments.

Image acquisition and analysis

Bright-field images were acquired using a Canon EOS Rebel XS digital SLR camera (Lake Success, NY). Other bright-field images were acquired using a Leica stereoscope. All fluorescence images were acquired by Leica DMI 6000 B epi-fluorescence microscope with a 5X / 0.15 NA objective and L5 filter at room temperature. All fluorescence images were corrected for background by using an image acquired with a standard fluorescent control slide. All the images were then stitched together using MetaMorph software (Molecular Devices, Sunnyvale, CA).

APPENDIX C

Authorship contribution statement and experimental section for Chapter 4

In the following publication

Sun, B.; Shen, F.; McCalla, S. E.; Kreutz, J. E.; Karymov, M. A.; Ismagilov, R. F., Mechanistic Evaluation of the Pros and Cons of Digital RT-LAMP for HIV-1 Viral Load Quantification on a Microfluidic Device and Improved Efficiency via a Two-Step Digital Protocol. *Anal. Chem.* **2013**, *85* (3), 1540-1546.

B.S. and R.F.I. designed the SlipChip experiments.

B.S. performed experiments and data analysis and was the lead researcher for all figures (Figure 9 to Figure 12 in this dissertation).

F.S. performed exploratory experiments for primer optimization.

S.E.M. performed ssDNA synthesis.

B.S., S.E.M., and R.F.I. wrote the paper.

J.E.K. contributed to the design of the two-step SlipChip and data analysis.

M.A.K. provided suggestions on experiment design and assisted the data acquisition for Figure 2 (Figure 9 in this dissertation).

Experimental section (as described in the publication above)

Chemicals and materials

All solvents and salts purchased from commercial sources were used as received unless otherwise stated. The LoopAmp® DNA amplification kit, the LoopAmp® RNA amplification kit, and the Calcein fluorescence indicator kit were purchased from SA Scientific (San Antonio, TX, USA). SsoFast EvaGreen Supermix (2X) was purchased from Bio-Rad Laboratories (Hercules, CA). Bovine serum albumin (BSA) and λ-DNA isolated from bacteriophage λ cl857 Sam 7 were purchased from Roche Diagnostics (Indianapolis, IN). Hybridase™ Thermostable RNase H was purchased from Epicentre Biotechnologies (Madison, WI). All primers were ordered from Integrated DNA Technologies (Coralville, IA). Mineral oil (D Nase, R Nase, and Protease free), tetradecane, and DEPC-treated nuclease-free water were purchased from Fisher Scientific (Hanover Park, IL). Dichlorodimethylsilane was purchased from Sigma-Aldrich (St. Louis, MO). AcroMetrix® HIV-1 Panel Copies/ml, EXPRESS One-Step SYBR® GreenER™ Universal, iPrepTM purification instrument, and iPrepTM PureLinkTM virus kit were purchased from Life Technologies (Grand Island, NY). PCR Mastercycler and in situ adapter were purchased from Eppendorf (Hamburg, Germany). Spectrum food color was purchased from August Thomsen Corp (Glen Cove, NY). Photomasks were designed in AutoCAD 2012 and ordered from CAD/Art Services, Inc. (Bandon, OR). Soda-lime glass plates coated with layers of chromium and photoresist were ordered from Telic Company (Valencia, CA). Polycarbonate SlipChip devices were designed in AutoCAD 2012 and purchased from microfluidic ChipShop GmbH (Jena, Germany).

Fabrication of SlipChips

Two-step exposing-etching protocol was adapted to create wells of two different depths (5 μm for thermal expansion wells, 55 μm for all the other wells). After etching, the glass plates were

thoroughly cleaned with piranha acid and DI water, and dried with nitrogen gas. The glass plates were then oxidized in a plasma cleaner for 10 minutes and immediately transferred into a desiccator for 1 hour of silanization. They were rinsed thoroughly with chloroform, acetone, and ethanol, and dried with nitrogen gas before use.

Plastic polycarbonate SlipChip devices were directly oxidized in a plasma cleaner for 15 minutes after they were received from microfluidic ChipShop GmbH, and then transferred into a desiccator for 90 minutes of silanization. They were soaked in tetradecane for 15 minutes at 65 °C and then rinsed thoroughly with ethanol, then dried with nitrogen gas before use. Plastic SlipChip devices were not reused.

Assembling and loading the SlipChips

The SlipChips were assembled under de-gassed oil (mineral oil: tetradecane 1:4 v/v). Both top and bottom plates were immersed into the oil phase and placed face to face. The two plates were aligned under a stereoscope (Leica, Germany) and fixed using binder clips. Two through-holes were drilled in the top plate to serve as fluid inlets. The reagent solution was loaded through the inlet by pipetting.

HIV viral RNA purification from AcroMetrix® HIV-1 Panel Copies/mL

400 μL plasma containing a modified HIV virus (5 million copies/mL, part of AcroMetrix® HIV-1 Panel Copies/mL) was loaded onto the iPrep™ PureLink® Virus cartridge. The cartridge was placed in the iPrep™ purification instrument and the purification protocol was performed according to the manufacturer's instructions. The elution volume was 50 μL. The purified HIV viral RNA was diluted 10, 102, 103 fold in 1 mg/mL BSA solution, aliquoted and stored at -80 °C for further use. HIV viral RNA purified from patient plasma was also aliquoted and stored at -80 °C upon receipt.

ssDNA synthesis

HIV cDNA was created by reverse transcription of the purified AcroMetrix® HIV RNA using the SuperScript III First-Strand Synthesis SuperMix according to the manufacturer's instructions. Briefly, a mixture of purified HIV RNA (10-fold diluted from the direct elution), 100 nM B3 primer, 1x Annealing buffer, and water were heated to 65 °C for 5 minutes and then placed on ice for 1 minute. A reaction mix and SuperScript III/RNase Out enzyme mix were added to the reaction for a final volume of 40 µL, and the mixture was placed at 50 °C for 50 minutes. The mixture was then heated to 85 °C for 5 minutes to deactivate the reverse transcriptase, chilled on ice, split into 5 µL aliquots, and frozen at -20 °C until further use. Biotin-labeled DNA was created in a PCR reaction containing a 1:50 dilution of the HIV cDNA, 500 nM biotin-B3 and F3 primers, 500 µM dNTPs, 1 U/µL Phusion DNA polymerase and 1x of the associated HF buffer mix. After an initial 1 minute enzyme activation step at 98 °C, the reaction was cycled 39 times at 98 °C for 10 s, 58 °C for 15 s, and 72 °C for 15 s, and finished with a 5 minute polishing step at 72 °C. The resulting DNA product was run on a 1.2% agarose gel in TBE buffer stained with 0.5 µg/mL ethidium bromide. The specific band was cut out and purified using the Wizard SV gel and PCR cleanup kit according the manufacturer's instructions and eluted into 50 µL of nuclease-free water. 50 µL of streptavidin MyOne T1 magnetic beads were primed by slow-tilt rotation for 24 hours in 20 mM NaOH14. The beads were washed 1 time with water and 4 times with binding buffer (5 mM Tris, 0.5 mM EDTA, 1 M NaCl, 0.05% Tween-20) and re-suspended in 30 µL of 2x concentrated binding buffer. 30 µL of PCR product was added to the beads and incubated for 15 minutes while gently rotating to allow binding of the DNA to the magnetic beads. The beads were separated with a magnet, the supernatant was removed, and the beads were re-suspended in 40 µL of 20 mM NaOH and incubated for 10 minutes on a rotator to separate the non-biotinylated strand. The beads were then separated with a magnet, and the supernatant containing the ssDNA was collected and mixed with 20 µL of 40 mM HCl. The resulting ssDNA was then purified

using an ssDNA/RNA cleaner and concentrator kit, eluted in 20 µL water, and run on an Agilent RNA nano bioanalyzer to confirm the size and integrity of the final product.

Primers used for RT-LAMP amplification and RT-PCR amplification

F3	ATTATCAGAAGGAGCCACC
B3	CATCCTATTTGTTCCTGAAGG
FIP	CAGCTTCCTCATTGATGGTCTCTTTTAACACCATGCTAAACACAGT
BIP	TATTGCACCAGGCCAGATGATTTTGTACTAGTAGTTCCTGCTATG
LOOPF	TTTAACATTTGCATGGCTGCTTGAT
LOOPB	GAGAACCAAGGGGAAGTGA

PCR_Forward: GRA ACC CAC TGC TTA ASS CTC AA

PCR_Reverse: GAG GGA TCT CTA GNY ACC AGA GT

dRT-LAMP and dLAMP amplification on SlipChip

To amplify HIV viral RNA using the one-step RT-LAMP method, the RT-LAMP mix contained the following: 20 µL RM, 2 µL BSA (20 mg/mL), 2 µL EM, 2 µL FD, 2 µL of primer mixture (20 µM BIP/FIP, 10 µM LooP_B/Loop_F and 2.5 µM B3/F3), various amount of template solution, and enough nuclease-free water bring the volume to 40 µL. The solution was loaded onto a SlipChip and heated at 63 °C for 60 minutes.

To amplify HIV viral RNA using the two-step RT-LAMP method, the first solution contained the following: 10 µL RM, 1 µL BSA, 0.5 µL EXPRESS SYBR® GreenER™ RT module (part of EXPRESS One-Step SYBR® GreenER™ Universal), 0.5 µL BIP primer (10 µM), various amount of, and enough nuclease-free water to bring the volume to 20 µL. The second solution contained: 10 µL RM, 1 µL BSA, 2 µL DNA polymerase solution (from LoopAmp® DNA amplification kit), 1 µL or 2 µL FD, 2 µL other primer mixture (20 µM FIP, 17.5µM FIP, 10 µM

LooP_B/Loop_F and 2.5 µM F3), 1 µL Hybridase™ Thermostable RNase H, and enough nuclease-free water to bring the volume to 20 µL. The first solution was loaded onto a SlipChip device and incubated at 37 °C or 50 °C, then the second solution was loaded onto the same device and mixed with the first solution, and the entire device was incubated at 63 °C for 60 minutes.

To amplify λ-DNA, the LAMP mix contained the following: 20 µL RM, 2 µL BSA (20 mg/mL), 2 µL DNA polymerase, 2 µL FD, 2 µL of primer mixture (20 µM BIP/FIP, 10 µM LooP_B/Loop_F and 2.5 µM B3/F3), various amount of template solution, and enough nuclease-free water to bring the volume to 40 µL. The same loading protocol as above was performed and the device was incubated at 63 °C for 70 minutes.

To amplify ssDNA, the LAMP mix contained the following: 20 µL RM, 2 µL BSA, 2 µL DNA polymerase, 2 µL FD, 2 µL of primer mixture (20 µM BIP/FIP, 10 µM LooP_B/Loop_F and 2.5 µM B3/F3), various amount of template solution, and enough nuclease-free water to bring the volume to 40 µL. The same loading protocol as above was performed and the device was incubated at 63 °C for 60 minutes.

dRT-PCR amplification on SlipChip

To amplify HIV viral RNA, the RT-PCR mix contained the following: 20 µL 2X Evagreen SuperMix, 2 µL BSA, 1 µL EXPRESS SYBR® GreenER™ RT module, 1 µL each primer (10 µM), 2 µL template, and enough nuclease-free water to bring the volume to 40 µL. The amplification was performed at the same conditions as reported before9 except for a shortened reverse transcription step of 10 minutes.

Image acquisition and analysis

The bright-field image and the fluorescence images in real-time dRT-LAMP experiments were acquired using a Leica MZ 12.5 Stereomicroscope. All other fluorescence images were acquired

using a Leica DMI 6000 B epi-fluorescence microscope with a 5X / 0.15 NA objective and L5 filter at room temperature unless stated otherwise. All the images were analyzed using MetaMorph software (Molecular Devices, Sunnyvale, CA).

APPENDIX D

Authorship contribution statement and experimental section for Chapter 5

In the following publication

Selck, D. A.; Karymov, M. A.; Sun, B.; Ismagilov, R. F., Increased Robustness of Single-Molecule Counting with Microfluidics, Digital Isothermal Amplification, and a Mobile Phone versus Real-Time Kinetic Measurements. *Anal. Chem.* **2013,** *85* (22), 11129-11136.

D.A.S, M.A.K. and B.S. contributed equally to this work.

D.A.S, M.A.K. and B.S. and R.F.I. designed the experiments and wrote the paper.

D.A.S performed all cell phone image acquisition with M.K., developed the software for data analysis, and assisted B.S. for in digital experiments.

B.S. performed all digital experiments and data acquisition with microscope analysis with Metamorph software.

M.K. was the lead researcher on Figure 3 and assisted cell phone image acquisition.

Experimental section (as described in the publication above)

Chemicals and materials

All solvents and salts purchased from commercial sources were used as received unless otherwise stated. The LoopAmp® DNA amplification kit, the LoopAmp® RNA amplification kit, and the Calcein fluorescence indicator kit were purchased from SA Scientific (San Antonio, TX, USA). SsoFast EvaGreen Supermix (2X) was purchased from Bio-Rad Laboratories (Hercules, CA). Bovine serum albumin (BSA) was purchased from Roche Diagnostics (Indianapolis, IN). Hybridase™ Thermostable RNase H was purchased from Epicentre Biotechnologies (Madison, WI). All primers were ordered from Integrated DNA Technologies (Coralville, IA). Mineral oil (DNase-, RNase-, and Protease-free), tetradecane, and DEPC-treated nuclease-free water were purchased from Fisher Scientific (Hanover Park, IL). Dichlorodimethylsilane was purchased from Sigma-Aldrich (St. Louis, MO). AcroMetrix® HIV-1 Panel Copies/ml, EXPRESS One-Step SYBR® GreenER™ Universal, iPrepTM purification instrument, and iPrepTM PureLink virus kit were purchased from Life Technologies (Grand Island, NY). PCR Mastercycler was purchased from Eppendorf (Hamburg, Germany). Eco real-time PCR system was purchased from Illumina, Inc. (San Diego, CA). Photomasks were designed in AutoCAD 2013 and ordered from CAD/Art Services, Inc. (Bandon, OR). Soda-lime glass plates coated with layers of chromium and photoresist were ordered from the Telic Company (Valencia, CA). Genomic DNA (Staphylococcus aureus, ATCC number 6538D-5) was purchased from American Type Culture Collection (Manassas, VA).

Fabrication, assembling and loading of SlipChip

The fabrication, assembling and loading protocol was the same as described in Appendix C.

Primers used for RT-LAMP amplification

F3	ATTATCAGAAGGAGCCACC
B3	CATCCTATTTGTTCCTGAAGG
FIP	CAGCTTCCTCATTGATGGTCTCTTTTAACACCATGCTAAACACAGT
BIP	TATTGCACCAGGCCAGATGATTTTGTACTAGTAGTTCCTGCTATG
LOOPF	TTTAACATTTGCATGGCTGCTTGAT
LOOPB	GAGAACCAAGGGGAAGTGA

dRT-LAMP amplification of HIV-1 RNA on SlipChip

The first solution, which was used for amplifying HIV-1 RNA using the two-step dRT-LAMP method, contained the following: 10 μL RM, 1 μL BSA, 0.5 μL EXPRESS SYBR® GreenER™ RT module (part of EXPRESS One-Step SYBR® GreenER™ Universal), 0.5 μL BIP primer (10 μM), various amounts of template, and enough nuclease-free water to bring the volume to 20 μL. The second solution contained 10 μL RM, 1 μL BSA, 2 μL EM (from LoopAmp® RNA amplification kit), 1 μL or 2 μL FD, 2 μL other primer mixture (20 μM FIP, 17.5 μM FIP, 10 μM LooP_B/Loop_F, and 2.5 μM F3), 1 μL Hybridase™ Thermostable RNase H, and enough nuclease-free water to bring the volume to 20 μL. The first solution was loaded onto a SlipChip device and incubated at 50 °C for 10 min, and then the second solution was loaded onto the same device and mixed with the first solution. The entire filled device was incubated at various temperatures (57 °C, 60 °C, or 63 °C) for 60 minutes.

Real-time RT-LAMP amplification of HIV-1 RNA

For two-step RT-LAMP amplification, a first solution containing the reagents described above was first incubated at 50 °C for 10 min and then mixed with a second solution, as described above. The 40 μL mixture was split into 4 aliquots and loaded onto an Eco real-time PCR machine. The amplification was performed at various temperatures (57 °C, 60 °C, or 63 °C) for 60 min. For one-step RT-LAMP amplification, the RT-LAMP mix contained the following: 20 μL RM, 2 μL

BSA (20 mg/mL), 2 µL EM, 2 µL FD, 2 µL of primer mixture (20 µM BIP/FIP, 10 µM LooP_B/Loop_F, and 2.5 µM B3/F3), various amount of template solution, and enough nuclease-free water bring the volume to 40 µL. The 40 µL mixture was split into 4 aliquots and loaded onto the Eco real-time PCR machine. The amplification was performed at various temperatures (57 °C, 60 °C, or 63 °C) for 60 min. Data analysis was performed using Eco software. To determine the reaction time (time required for the fluorescent signal to cross the threshold), fluorescence intensity between 5 min and 15 min was used as the baseline and the threshold value was set to be 2.

Microscope image acquisition and analysis

Fluorescence images of each device were acquired using a Leica DMI 6000 B epi-fluorescence microscope with a 5X / 0.15 NA objective and L5 filter at room temperature. All the images were analyzed using MetaMorph software (Molecular Devices, Sunnyvale, CA). Images taken in each experiment were stitched together and a dark noise background value of 110 units was subtracted before the image was thresholded. The number of positive wells was automatically counted using the integrated morphology analysis tool based on intensity and pixel area. Typical arbitrary fluorescence values for the negative wells were 80 ± 10. Arbitrary fluorescence values for the positive wells were largely centered around 350 ± 100.

Cell phone camera setup and settings

A Nokia 808 Pureview cell phone was used to image and count microwells containing the amplification product. This cell phone features a CMOS sensor with a Xenon flash. The Nokia 808 uses a 1/1.4-inch 41-megapixel sensor with a pixel size of 1.4 µm. The camera has a Carl Zeiss F2.4 8.02 mm lens and contains a set of “PureView” modes which are able to combine multiple pixels by using pixel oversampling, thus increasing an individual pixel’s area (which, consequently, lowers the image’s resolution). This feature increases the sensitivity of each

individual pixel in the final image. Since the shortest focal length of the camera's lens is 15 cm, we used a non-branded, commercially available 0.67 x magnetically mounted wide lens designed for iPhone. Using this objective, we were able to obtain images at a distance of 6.5 cm from the device, which effectively increased the total number of photons collected from the device, thus improving camera sensitivity. A set of filters was used for both excitation and emission purposes. To improve filtering, one additive dichroic filter (model number FD1B, Thorlabs, Newton, NJ) was cut in half and the two halves were stacked and attached to the camera. For fluorescence detection, two 5CGA-530 long-pass filters (Newport, Franklin, MA) were inserted into magnetically mounted lens. The imaging process with a cell phone was performed with the device tilted at 10 degrees relative to the cell phone plane to prevent direct reflection of the flash to the lens. This was achieved by placing the device on a tilted glass slide (3" x 2") that had been painted black on the bottom side to reduce background noise. Tetradecane was placed in between the device and the slide to reduce glare. All images were taken using the stock camera application. The white balance was set to automatic, the ISO was set at 800, the exposure value was set at +2, the focus mode was set to "close-up," and the resolution was adjusted to 8 MP.

Real-time dRT-LAMP imaging and analysis

Time traces of dRT-LAMP reactions were obtained by imaging a progressing dRT-LAMP reaction every minute using a Leica MZFLIII stereomicroscope. This was performed by placing an Eppendorf mastercycler with an in-situ adapter plate within the imaging field of the stereoscope. The stereoscope was set to a magnification of 1X and placed in such a way that it could move relative to the position of the thermocycler. At each required time-point, a fluorescent image of one-half of the device was taken, and then the stereoscope was moved to image the second half of the device. The camera attached to the stereoscope was a Diagnostic Instruments color mosaic model 11.2 camera and images were acquired using Spot imaging software. The imaging was done with a gain of 4 and an exposure time of 2 seconds. The acquired images were

then analyzed using the ImageJ software package. The images were manually edited to remove wells that appeared in both images, after which, the green color plane was extracted and a threshold value of 30 was applied. The binary image was then filtered to keep all spots within an area between 65 and 350 leaving the number of positive wells. After performing this analysis with images comprising both halves of the device, the numbers for each half were added together, yielding the total number of positive wells at that specific time point.

Statistical analysis of data sets obtained at different temperatures

The t-test is used to evaluate whether the means of two different data sets are statistically different. The p value obtained in this process is the probability of obtaining a given result assuming that the null hypothesis is true. A 95% confidence level, which corresponds to $p = 0.05$, or a 5% significance level, is commonly acceptable. It is typically assumed that the concentrations of two samples are different when $p < 0.05$. Here, we used a p value to evaluate the performance of two-step dRT-LAMP in various imaging conditions—with a microscope, with a cell phone and a shoe box, and with a cell phone in dim lighting. When we pooled all data for one concentration from different temperatures and compared them to data acquired at another concentration, the highest p value among the three imaging conditions was 6.7 x 10-7. Thus, the two concentrations were clearly distinguishable and the null hypothesis, which stated that both concentrations were equivalent, was rejected. We also compared the two closest subsets (2 x 105 copies/mL at 57 °C and 1 x 105 copies/mL at 63 °C) and calculated their p-value under each set of imaging conditions. The p-values were still below 0.05 for all three conditions. Additionally, we used normal distributions as visual guides for data interpretation. We can use normal distributions instead of theoretical t-distributions because we determined standard deviations from the data. There was no visible overlap between the data sets corresponding to the two concentrations.

Cloud-based automatic analysis

The Symbian software on which the Nokia 808 cell phone is based can access Skydrive, a cloud-based storage service produced by Microsoft. This service can automatically upload images to the cloud for storage directly after imaging, without any user intervention. Almost instantly, those uploaded files are synced with all other computers running Skydrive that are logged in to the same account, and the images can be analyzed on multiple computers. Here, we used a secondary computer with a custom Labview program, including a built-in "file watcher" function whereby all files added to a specific directory that fell within a specific filtered category (i.e., *.jpg) were automatically analyzed. The analysis of images included a multi-step algorithm. First, the RGB color image was split into three monochrome 8-bit images for each individual color. The red-channel image was used to determine whether or not the entire chip had been imaged by searching for markers on the device (four red circles of tape, in this case). If all circles had been found, the image was then rotated such that the device was parallel to the top of the image box, removing any rotational bias. A background-corrected image was then generated by subtracting the red-channel monochrome image from the green-channel monochrome image, which contained the fluorescence information. The image was then subjected to a filtering process to increase the intensity of the positive wells. The filtering process included the following steps, in the following order: i) a 3 x 3 "local average" filter, ii) a 2 x 2 "median" filter, iii) an 11 x 11 "highlight details" filter, and iv) a 5 x 5 "median" filter. The filtered image was then thresholded using an entropy algorithm. After thresholding, a portion of the image (defined by the position of the markers) was analyzed and all individual spots were subjected to a size-filtering algorithm. This yielded the eventual total number of counts, which was then statistically transformed into a concentration before being emailed to the user or proper authority.

APPENDIX E

Authorship contribution statement and experimental section for Chapter 6

In the following publication

Bing Sun, Jesus Rodriguez-Manzano, David A. Selck, Eugenia Khorosheva, Mikhail A. Karymov, and Rustem F. Ismagilov, "Measuring Fate and Rate of Single-Molecule Competition of Amplification and Restriction Digestion, and Its Use for Rapid Genotyping Tested with Hepatitis C Viral RNA" *Angew. Chem. Int. Ed.* **2014**, accepted.

B.S, J.R.M and R.F.I developed the idea, designed the experiments and prepared the manuscript.

B.S and J.R.M contributed equally.

B.S and J.R.M led and performed the experiments and the data analysis (Figure 17 to Figure 21 in this dissertation).

D.A.S built the real-time digital instrument and helped image enhancement.

E.K and M.A.K performed the HCV RT-LAMP primer design and optimization based on previous publication, which was further optimized by J.R.M.

Experimental section (as described in the publication above)

Chemicals and materials

All solvents and salts purchased from commercial sources were used as received unless otherwise stated. The Loopamp® RNA amplification kit and the Loopamp® Fluorescent Detection Reagent kit were purchased from SA Scientific (San Antonio, TX, USA). The LoopAmp® RNA amplification kit contains 2X Reaction Mix (RM) (40 mM Tris-HCl pH 8.8, 20 mM KCl, 16 mM MgSO4, 20 mM (NH4)2SO4, 0.2% Tween20, 1.6 M Betaine and dNTPs 2.8 mM each), Enzyme Mix (EM) (mixture of Bst DNA polymerase and AMV reverse transcriptase), and distilled water (DW). Loopamp® Fluorescent Detection Reagent kit contains Fluorescent Detection Reagent (FD) (including calcein). SsoFast EvaGreen Supermix (2X) was purchased from Bio-Rad Laboratories (Hercules, CA). Bovine serum albumin (BSA) was purchased from Roche Diagnostics (Indianapolis, IN). All restriction enzymes were purchased from New England Biolabs (Ipswich, MA). All primers were ordered from Integrated DNA Technologies (Coralville, IA). Mineral oil (DNase, RNase, and Protease free), tetradecane, and DEPC-treated nuclease-free water were purchased from Fisher Scientific (Hanover Park, IL). Dichlorodimethylsilane was purchased from Sigma-Aldrich (St. Louis, MO). AcroMetrix® HCV-s panel and AcroMetrix® HCV High Control and EXPRESS One-Step SYBR GreenER Universal were purchased from Life Technologies (Grand Island, NY). Genotype 3 and genotype 4 HCV viral isolates were purchased from SeraCare Life Sciences (Gaithersburg, MD). Nucleic acid extraction kit QIAamp Viral RNA Mini kit was purchased from QIAGEN (Inc, Valencia, CA, USA) PCR Mastercycler and in situ adapter were purchased from Eppendorf (Hamburg, Germany). Eco real-time PCR system was purchased from Illumina, Inc. (San Diego, CA). Photomasks were designed in AutoCAD 2013 and ordered from CAD/Art Services, Inc. (Bandon, OR). Soda-lime glass plates coated with layers of chromium and photoresist were ordered from the Telic Company (Valencia,

CA). Sanger sequencing service was provided by Laragen, Inc. HCV sequences were extracted from Los Alamos database and aligned with Geneious software.

HCV isolates in plasma

We assayed 4 different HCV genotypes. Genotypes 1 and 2 were purchased from Acrometrix Corporation (Benicia, CA, USA) and genotypes 3 and 4 from SeraCare Life Sciences (Milford, MA, USA). Genotype and viral load information was provided by these companies: viral load of 2.5×107 IU/mL for GT1, 1.1×106~3.4×106 IU/mL for GT2, 5.7×106 IU/mL for GT3, and 4.97×106 IU/mL for GT4. The genotype information was also provided by the companies and we confirmed the genotype by sequencing and phylogenetic analysis. The presence of targeted single-nucleotide polymorphisms or SNPs (restriction enzyme cutting sites) was confirmed by manual inspection of the sequencing chromatograms.

RNA extraction from HCV isolates

RNA was extracted using the QIAamp Viral RNA Mini Kit (QIAGEN Inc, Valencia, CA, USA) according to the manufacturer's instructions, using 200 μL of plasma and eluting the resulting nucleic acid extraction in 60 μL of elution buffer. Nucleic acid extractions were analyzed immediately or stored at -80 °C until further analysis.

Preparing DNA for sequencing using RT-PCR

To amplify HCV viral RNA, the RT-PCR mix contained the following: 20 μL of 2X SsoFast Evagreen SuperMix, 1 μL of EXPRESS SYBR GreenER RT module, 1 μL of each primer (10 μM), 2 μL of template, and enough nuclease-free water to bring the volume to 40 μL. The reverse transcription was carried out at 50 °C for 15 min, followed by 2 min of reaction termination at 95 °C. The amplification step was performed by 40 cycles of the following conditions: 95 °C for 15 seconds, 55 °C for 1 min and 72 °C for 1 min.

Phylogenetic analysis

The dendogram was constructed by alignment of the 222 nucleotide sequences within the UTR region of HCV based on the UPGMA method under the Tamura-Nei model (bootstrap = 1,000 replicates). Reference sequences from HCV strains (genotypes 1 to 4) were obtained from the Los Alamos HCV database.

Primers used for RT-LAMP

F3	CCTCCCGGGAGAGCCATAG;
B3	GCACTCGCAAGCACCITATC
FIP	TCCAAGAAAGGACCCIGTCTTTTTCTGCGGAACCGGTGAGTAC
BIP	TTGGGCGTGCCCCCGCIAGATTTTTCAGTACCACAAGGCCITTCGCIACC
LOOPF	TTICCGGIAATTCCGGT
LOOPB	CTGCTAGCCGAGTAGIGTTG

Real-time bulk RT-LAMP/RE competition assay

To amplify HCV viral RNA using RT-LAMP on a real-time PCR machine, the RT-LAMP mix contained the following: 20 μL of 2X reaction mix (RM), 2 μL of enzyme mix (EM), 1 μL of fluorescent detection reagent (FD), 4 μL of primer mixture (20 μM BIP/FIP, 10 μM LooP_B/Loop_F, and 2.5 μM B3/F3), various amounts of RNA template solution, and enough nuclease-free water to bring the volume to 40 μL. The solution was split into 10 μL each and loaded into 3 wells on the Eco real-time PCR plate and heated at 63 °C for 50 min. RT-LAMP reagents and FD were used as purchased from SA Scientific and used as it was.

To amplify HCV viral RNA using RT-LAMP in the presence of RE on real-time PCR machine, the RT-LAMP mix contained the following: 20 μL of RM, 2 μL of EM, 1 μL of FD, 4 μL of primer mixture (20 μM BIP/FIP, 10 μM LooP_B/Loop_F, and 2.5 μM B3/F3), various amounts

of RNA template solution, 4 μL 20-fold diluted RE (to make a 200-fold dilution in the final solution) and enough nuclease-free water to bring the volume to 40 μL. RE was diluted in nuclease-free water before immediately mixed with RT-LAMP reagents, and fresh dilution was made each time. The solution was split into 10 μL each and loaded into 3 wells on the Eco real-time PCR plate and heated at 63 °C for 50 min.

Real-time bulk RT-LAMP/RE data analysis

Bulk RT-LAMP/RE assays were carried out in an Eco Real-Time PCR System (Illumina, SD, USA) and data analysis was performed using Eco Real-Time PCR System Software (version 4.0). To determine the time-to-positive (time required for the fluorescent signal to cross the threshold), fluorescence intensity between 5 min and 15 min was used as the baseline and the threshold value was set to be half height of the maximum intensity.

Fabrication of SlipChip

The single-volume 1280-well SlipChip was designed and optimized based on previous work. The procedure of fabricating SlipChip from soda-lime glass was based on the procedure described in previous work. All features were etched to a depth of 55 μm to make the volume of loading well equal to 3 nL. The cleaning, assembling and loading protocol was same as described in other chapters.

Real-time digital competition assay on SlipChip

To amplify HCV viral RNA using RT-LAMP method on real-time PCR machine, the RT-LAMP mix contained the following: 20 μL of RM, 2 μL of EM, 1 μL of FD, 4 μL of primer mixture (20 μM BIP/FIP, 10 μM LooP_B/Loop_F, and 2.5 μM B3/F3), 2 μL of BSA (20 mg/mL), various amounts of RNA template solution, 4 μL diluted RE if not for positive control, and enough nuclease-free water to bring the volume to 40 μL. The solution was loaded onto SlipChip and

heated at 63 °C for 50 min on a custom-built real-time instrument. RT-LAMP reagents and FD were used as purchased from SA Scientific. BSA was used as purchased from Roche Diagnostics.

Custom-built real-time instrument imaging

Experiments were performed on a Bio-Rad PTC-200 thermocycler with a custom machined block. The block contains a flat 3” x 3” portion onto which the devices are placed ensuring optimal thermal contact. The excitation light source used was a Philips Luxeon S (LXS8-PW30) 1315 lumen LED module with a Semrock filter (FF02-475). Image Acquisition was performed with a VX-29MG camera and a Zeiss Macro Planar T F2-100mm lens. A Semrock filter (FF01-540) was used as an emission filter.

Data analysis using Labview software

Images acquired were analyzed using self-developed Labview software. The data were analyzed by first creating a binary mask that defined the location of each reaction volume within the image. The masked spots were then overlaid on the stack of images collected over the course of the experiment and the average intensity of each individual masked spot was tracked over the course of the stack. Background subtraction of the real-time trace was performed by creating a least mean square fit of each individual trace. Threshold was then manually set at the half height of the averaged maximum intensity, and the time-to-positive of each reaction was then determined as the point at which the real-time curve crossed the defined threshold.

Cell phone imaging protocol

Cell phone imaging setup was the same as previously described. The white balance was set to automatic, the ISO was set at 800, the exposure value was set at +2, the focus mode was set to “close-up”, and the resolution was adjusted to 8 MP.

DNA gel electrophoresis analysis of RE digestion of amplified RT-LAMP product

To test the specificity and activity of RE at the condition for RT-LAMP, we first prepared RT-LAMP product from HCV RNA of genotype 1, 2, 3, and 4, respectively. The amplification procedure was the same as described in “Real-time bulk RT-LAMP/RE competition assay” except that an additional 5 min at 85 ℃ was used to inactivate the polymerase. 2 µL RT-LAMP product was mixed with 4 µL fresh RM, 3 µL nuclease-free water and 1 µL RE (or water for non-RE control) and incubated at 63 ℃ for 30 min. The digestion product was analyzed on 1.2% agarose DNA gel stained with ethidium bromide at 75 Volt for 40 min.

APPENDIX F

Poisson statistics in the context of digital PCR.

Reprinted with permission from reference 23. Copyright 2011 American Chemical Society.

Poisson analysis of single-volume PCR:

There are two key assumptions that need to be maintained in order for digital PCR methods and analysis to accurately quantify nucleic acid concentrations: 1) Having at least one target molecule in a well is necessary and sufficient for a positive signal and 2) Target molecules do not interact with one another or device surfaces, to avoid biasing their distribution. At the simplest level of analysis, when molecules are at low enough densities that there is either 0 or 1 molecule within a well, concentrations can be estimated simply by counting positives. However, if the two key assumptions above hold true, then Poisson and binomial statistics can be used to obtain quantitative results from experiments resulting in one positive well to experiments resulting in one negative well. The Poisson distribution (Eq. 1), in the context of digital PCR, gives the probability, *p*, that there are *k* target molecules in a given well based on an average concentration per well, $v \cdot \lambda$, where v is the well volume (mL) and λ is the bulk concentration (molecules/mL). In digital PCR, the same readout occurs for all k>0, so if k=0 then Eq. 1 simplifies to give the probability, *p*, that a given well will not contain target molecules (the well is "negative").

$$p = \left((v \cdot \lambda)^k \cdot e^{-(v \cdot \lambda)}\right) / k!, \text{ and for k=0 (empty well), } p = e^{-(v \cdot \lambda)} \quad (1)$$

In single-volume systems, the number of negative wells, *b*, out of total wells, *n*, can serve as an estimate for *p*, so expected results can be estimated from known concentrations, or observed results can be used to calculate expected concentrations (Eq. 2).

$$b = n \cdot e^{-(v \cdot \lambda)} \text{ or } \lambda = -\ln(b/n)/v \quad (2)$$

The binomial equation is used to determine the probability, *P*, that a specific experimental result (with a specific number of negatives, *b*, and positives, *n*-*b*, out of the total number of wells, *n*, at each volume) will be observed, based on λ (Eq. 3), where $\binom{n}{b} = \frac{n!}{b!(n-b)!}$.

$$P = \binom{n}{b} \cdot p^b \cdot (1-p)^{n-b} \text{ or } P = \binom{n}{b} \cdot \left(e^{-v \cdot \lambda}\right)^b \cdot \left(1 - e^{-v \cdot \lambda}\right)^{n-b} \quad (3)$$